universität wien

MASTERARBEIT / MASTER'S THESIS

Titel der Masterarbeit / Title of the Master's Thesis

„Like ships that pass in the night:
Coma Berenices and its neighbor moving group“

verfasst von / submitted by

Verena Fürnkranz, BSc

angestrebter akademischer Grad / in partial fulfilment of the requirements for the degree of

Master of Science (MSc)

Wien, 2019 / Vienna 2019

Studienkennzahl lt. Studienblatt / degree programme code as it appears on the student record sheet:	A 066 861
Studienrichtung lt. Studienblatt / degree programme as it appears on the student record sheet:	Masterstudium Astronomie
Betreut von / Supervisor:	Dr. Stefan Meingast, Bakk. MSc

"Ships that pass in the night,
and speak each other in passing,
only a signal shown,
and a distant voice in the darkness;
So on the ocean of life,
we pass and speak one another,
only a look and a voice,
then darkness again and a silence."

— Henry Wadsworth Longfellow —

Acknowledgements

I would not have been able to study Astronomy without having the support of my family. Thank you Papa for making my dream possible, thank you Mama for being excited about everything I do, and thank you Petra for being my (most favorite) sister.

I am very fortune to have a person by my side who makes it through everything with me. Thank you Lukas for being the constant in my life, and for making me incredibly happy every day.

I would like to thank all my colleagues and friends who made my student days the best time of my life. Thank you for helping me whenever I needed help, and thank you for so many memorable moments outside of university.

I could not have done anything better than joining the group of João Alves for my master project. Thank you João for always being enthusiastic about my work, and for always being kind, supportive, and encouraging. Thank you for showing me the science and research world, and thank you for being - scientifically and personally - a great example to me.

Last but not least, I feel greatly privileged to have been advised by Stefan Meingast. Thank you Stefan for the incredible large amount of time you spent helping me with my work. Thank you for your hours of explanation, for helping me improving my skills, and for always (!) having time for me and my problems. I enjoyed working (and having coffee breaks) with you a lot. My fascination and enthusiasm for astronomy could not be greater, and you have largely contributed to this. Thank you for everything.

Abstract

Open star clusters and associations are excellent tracers to study the formation, evolution, and structure of the Galactic disk. A key characteristic of open clusters is their small velocity dispersion. Therefore, they appear as small-scale velocity structures in the Milky Way, and their investigation delivers insights into e.g. the dynamical evolution of star clusters in tidal fields, star cluster disruption and mass loss, the build-up of the Galactic field population, and the mass distribution of the Galactic disk. The second *Gaia* data release provides astrometric data with a precision we have never had before. Its accurate position and velocity measurements enable new insights into the properties of stellar populations in the Galactic disk and contribute greatly to revolutionizing our knowledge about the Milky Way.

This thesis studies the well-known open cluster Coma Berenices and a previously unknown moving group of stars in its velocity and spatial neighborhood. The new group identified in tangential velocity space as measured by *Gaia* contains at least 177 coeval members distributed in two subgroups, and appears as a flattened structure parallel to the plane, stretching for about 50 pc. More remarkably, the new group, which appears to have formed about 300 Myr later than Coma Berenices in a different part of the Galaxy, will share essentially the same volume with the older cluster when the centers of both groups will be at their closest in 13 Myr. This will result in the mixing of two unrelated populations with different metallicities. The phase of cohabitation for these two groups is about 20 - 30 Myr, after which the two populations will drift apart. We estimate that temporal cohabitation of such populations is not a rare event in the disk of the Milky Way, and of the order of once per Galactic revolution. Our study also unveils the tidal tails of the Coma Berenices cluster, an effect of cluster disruption due to the tidal field of the Milky Way.

Contents

Acknowledgements iii

Abstract v

1. Introduction 1

1.1. Open clusters and associations . . . 1

1.1.1. General properties . . . 1

1.1.2. Formation of open clusters . . . 4

1.1.3. Evolution of open clusters . . . 7

1.2. Contribution of *Gaia* . . . 12

1.3. Motivation and goal of the thesis . . . 15

2. Methods description 17

2.1. Calculation of galactic coordinates and velocities . . . 17

2.2. Galactic dynamics . . . 20

2.2.1. Orbit integration with Galpy . . . 21

2.2.2. Uncertainties and errors of orbital parameters . . . 22

2.3. Cluster membership determination . . . 24

2.3.1. Clustering with DBSCAN and k-NN algorithm . . . 24

2.3.2. Contamination fraction estimate . . . 28

3. Coma Berenices and its neighbor moving group 31

3.1. Overview . . . 31

3.2. Publication details . . . 31

3.3. Introduction . . . 32

3.4. Data description and member selection . . . 32

3.5. Results and discussion . . . 33

3.5.1. Structure . . . 33

3.5.2. Age and metallicity . . . 34

3.5.3. Kinematics and Galactic orbit . . . 34

3.6. Summary and conclusions . . . 35

3.7. References . . . 36

3.8. Appendix A: Supplementary plots and tables . . . 37

4. Conclusions and Outlook **39**
4.1. Summary of results 39
4.2. Discussion and future work 39

References **42**

A. Appendix **53**
A.1. Zusammenfassung 55
A.2. List of Figures 57
A.3. Reprint permission 59

1. Introduction

The universe is a pretty large mystery, and we enrich our knowledge about it step by step, gradually studying its components, longing to increase our insights into the processes and mechanisms that make its presence and our existence possible.

The aim of this work is to study open clusters and associations, stellar components of the Milky Way's disk, as they deliver insights into the structure of our Galaxy, and contribute to our knowledge of its formation and evolution.

1.1. Open clusters and associations

A star cluster is a group of stars held together by gravitational forces. The stars belonging to a star cluster were born in the same molecular cloud, and therefore share the same age and chemical composition. They are located at approximately the same distance from the Sun, and orbit the center of the Galaxy. The Milky Way is home to billions of stars and thousands of star clusters. Therefore, in order to understand the formation, structure, and evolution of our home galaxy, it is key to study the properties, formation, and evolution of its star clusters.

As stated in Castro-Ginard et al. (2018b), the investigation of young open clusters delivers insights into the formation mechanism of stars, e.g. the star formation efficiency, the fragmentation of the cloud, and the IMF. Furthermore, young star clusters are excellent tracers for star forming regions, because they are located not far away from their parent molecular clouds. By studying the evolution of open clusters, especially the continuous evaporation of cluster stars into the field, they deliver hints to the build-up of the Galactic field star population. Old open clusters allow to study the chemical enrichment of the Galactic disk. In addition, open clusters are key to study stellar evolution and dynamical interactions between stars, and are excellent tracers to study the formation, evolution and structure of the Galactic disc, as well as the Galaxy's spiral arm structure.

1.1.1. General properties

We distinguish between two main types of star clusters, namely the open clusters[1] and the globular clusters. Globular clusters orbit the Galactic center in the halo of the Galaxy. They contain tens of thousands to hundreds of thousands of stars, are very

[1] Due to their location in the Galactic disk, they are often referred to as 'galactic clusters'.

(a) Messier 80 (b) Pleiades

Figure 1.1.: Comparison between Messier 80, an old far and massive globular cluster (a), and the Pleiades, a young nearby, and less massive open cluster (b). Credit: Hubble Heritage Team/Antonio Fernandez-Sanchez

tightly bound by gravity, and show a spherical shape. They are among the oldest objects associated with the Galaxy and show very low metallicity. On the other hand, open clusters are concentrated close to the Galactic disk. They have up to a few hundred member stars, are very loosely gravitationally bound and can have an irregular shape. They are very young, typically between a few tens up to a few hundred million years old, and their member stars have a higher metallicity than globular clusters. Open clusters are only found in spiral and irregular galaxies where star formation is still ongoing, whereas globular clusters are also present in elliptical galaxies.

Figure 1.1 shows two stellar clusters associated with the Milky Way. The globular cluster Messier 80 is located at a distance of about 10 kpc, has an age of approximately 12.5 billion years, and is dominated by several hundred thousand stars with very low masses. Due to their low temperatures, they appear to shine in red, orange, and yellow. On the other hand, the Pleiades open cluster, with a distance of approximately 136 pc one of the closest clusters to the Sun, has an age of only about 100 million years, and contains many massive, hot stars, which therefore appear to shine in white and blue.

Another type of stellar groups are the so-called stellar associations. The stars of stellar associations were born together and are still moving together in space, but appear as very loose groupings, because they are not gravitationally bound. They are not easy to detect, because they hardly stand out against background field stars. In the past, it has often been stated that associations are the result of star cluster dispersal over time.

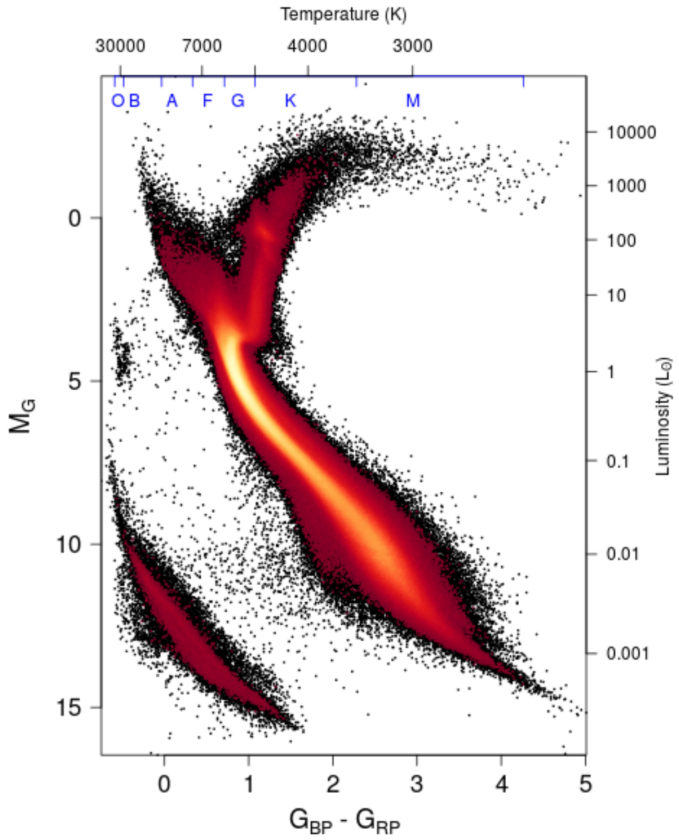

Figure 1.2.: Observational Hertzsprung-Russel diagram of *Gaia* DR2 sources. Credit: Gaia Collaboration et al. (2018a)

However, recent work shows that they most likely already formed in-situ as extended low-density structures (Wright, 2018; Ward et al., 2019). An attempt to physically define whether a population is a bound cluster or a loose association was done by Gieles and Portegies Zwart (2011). They compare the age of the stars to the crossing time of stellar groups. According to their work, stellar groups for which the age of the stars exceeds the crossing time are referred to as bound clusters, whereas those for which the crossing time exceeds the stellar age are referred to as unbound associations (Gieles and Portegies Zwart, 2011).

A very powerful diagnostic tool in astronomy is the Hertzsprung-Russel diagram. Figure 1.2 shows a Hertzsprung-Russel diagram for stars in the *Gaia* DR2 catalogue, the colorscale corresponds to the source density in the plot. It demonstrates the relation between the temperature/spectral type and the absolute magnitude of stars, and represents an important tool for studying stellar evolution. In this diagram, the temperature decreases from left to right, and the luminosity increases from bottom to top, which indicates that hot bright stars are located at the upper left corner of the diagram, and

cool faint stars appear in the bottom right corner. The densest region is the main sequence, which is a diagonal lane from the upper left to the lower right part. Different evolutionary stages are clearly separated, e.g. white dwarfs appear in the bottom left corner, and giants and subgiants are located above the main sequence. The location of a star in this diagram provides information about its present evolutionary stage and mass. As stars change their temperature and luminosity during their lifetimes, they also change their position in the diagram.

Stellar clusters are key to improve our knowledge of stellar evolution, which is a difficult task as this takes place on billion-year time scales. Stellar clusters contain stars with similar ages, chemical composition and distance, but present a wide range of masses. If all stars of a star cluster plotted in a Hertzsprung-Russel diagram show a narrow sequence, they likely have a similar age and chemical composition. The so-called turn-off point for a star shows where it leaves the main sequence, which depends on the stellar mass. Thus, we can estimate the age of a stellar population by determining the main sequence turn-off, where older clusters show a turn-off at lower luminosities and temperatures. Therefore, star clusters are an important basis for stellar age determination via isochrones. Isochrones are lines in a Hertzsprung-Russel diagram and represent stellar populations with equal ages. On one hand, we need star clusters to obtain these isochrones, in order to estimate ages. In turn, we can then use these isochrones to determine the ages of other star clusters.

1.1.2. Formation of open clusters

Most stars are born in clusters[2] (Lada and Lada, 2003). Their birthplaces are dense and cold (T = 10-20 K) molecular clouds, which consist mainly of molecular hydrogen (H_2). Initially, these clouds are in an equilibrium state, where the gas pressure stabilizes the cloud against gravitational forces. Small perturbations (e.g. cloud-cloud collisions, nearby supernova explosions, galaxy interactions, shockwaves from spiral arms) can initiate a gravitational contraction of the cloud, which is stronger than the internal thermal gas pressure, and leads to a collapse of the cloud. The so-called Jeans-mass (M_J) is the critical mass, above which the cloud becomes gravitational unstable (Jeans, 1902).

$$M_J \propto T^{2/3} \rho^{-1/2} \tag{1.1}$$

[2]We use the term 'cluster' for an enhancement over the background, not for a gravitational bound structure.

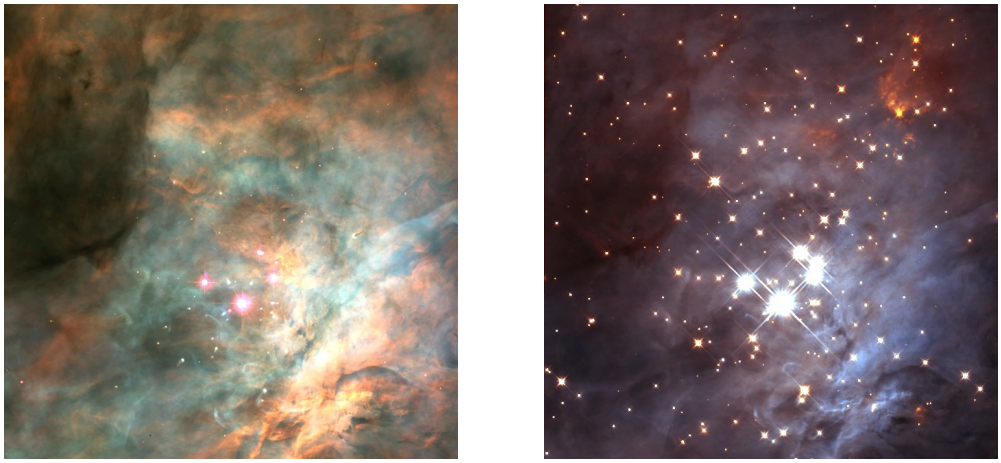

(a) Visible light (b) Near infrared

Figure 1.3.: The embedded cluster Trapezium, observed in different wavelengths by the Hubble space telescope. Due to the surrounding gas and dust, the newborn stars are hardly visible in optical wavelengths, but become visible in the IR. Credit: NASA/ESA

As can be seen in Equation 1.1, the mass limit is lower if the temperature is lower or the density is higher, which makes cold and dense molecular clouds ideal birthplaces for stars.

As the cloud contracts, the density rises, but due to cooling processes in the cloud, the temperature remains constant at first (isothermal collapse). This decreases the mass limit of the Jeans-criterion, and subsequently small initial density inhomogeneities become unstable as well, and individual regions start to collapse independently. This process is called fragmentation. The cores in the middle of the fragments become denser and hotter, until nuclear fusion starts. The pressure from nuclear fusion starts to act against the gravitational force, which stabilizes the system. The typical timescale for star formation is very short and estimated to last for about 1 Myr.

After their formation phase, the new born stars remain (fully or partially) embedded in their natal molecular cloud during their first 2-5 million years. Figure 1.3 shows that these so-called embedded clusters are difficult to observe at optical wavelengths, because they are surrounded by gas and dust, but become visible through infrared observations. These embedded clusters are the progenitors of open clusters. However, according to Lada and Lada (2003), about 90% of them disrupt at early stages, because we observe a 10 times lower number of open clusters than embedded clusters. The fact that only 10% of the clusters survive their parent molecular cloud is called infant mortality, and the main driving mechanism responsible for their early destruction is gas expulsion: stellar

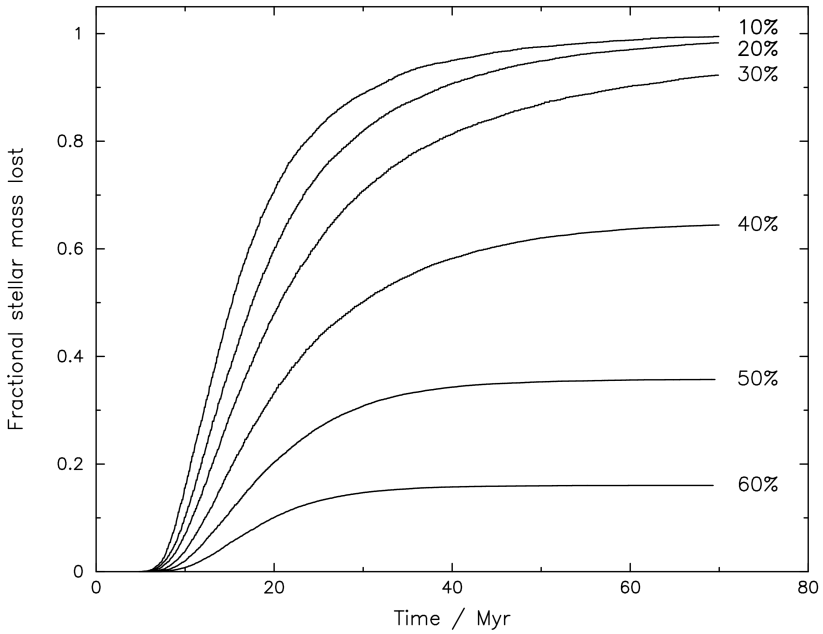

Figure 1.4.: The fraction of stellar mass which is lost due to rapid gas expulsion, as a function of time for different star formation efficiencies. For SFE's <30%, the cluster disrupts. For SFE's >30%, the cluster manages to retain a bound core, but still loses a huge fraction of its mass. Credit: Goodwin and Bastian (2006)

feedback (e.g. massive stellar winds, radiation pressure, supernovae) drives out the gas which was not used for star formation, and disrupts the young star clusters.

Several parameters are important to determine whether gas expulsion destroys an embedded cluster (Lada and Lada, 2003; Baumgardt and Kroupa, 2007). One fundamental parameter is the star formation efficiency (SFE), which is the fraction of gas that is converted into stars. Star formation is a very inefficient process, and observations of embedded clusters reveal typical values of only about 10-30%, in reference to dense gas (Alves et al., 2007). The overall star formation efficiency in giant molecular clouds is only of order 1-3% (Lada, 2005). In addition, the timescale for gas removal determines how disruptive gas expulsion acts. Figure 1.4 shows the fraction of stellar mass which is lost due to rapid gas expulsion, as a function of time for different star formation efficiencies. If the gas removal is fast (< crossing time), then all clusters with a SFE < 30% are destroyed (Goodwin and Bastian, 2006). If the gas removal is slow (> crossing time), the effects of gas loss are less dramatic, and lower SFE's are possible. Furthermore, the cluster lifetime is determined by its mass. Those clusters that survive gas expulsion and violently relax into an equilibrium state are likely to be the most massive ones, with an embedded cluster mass of $M_{EC} \geq 500\ M_{\odot}$ (Lada and Lada, 2003). However, taking

only SFE, gas removal time, and cluster mass into account seems to be a simplification of the processes (Pelupessy and Portegies Zwart, 2012). Simulations, which take more parameters into account (e.g. an external tidal field or the virial state of clusters before gas expulsion (Baumgardt and Kroupa, 2007; Goodwin, 2009) show that - depending on the conditions - even star clusters with SFE = 5% might even be able to survive. However, work done by Kruijssen (2012) shows that gas expulsion does not destroy embedded clusters in general. As stated in his work, gas expulsion does not affect the formation of bound clusters which are born in high-density regions and achieve high star formation efficiencies, but significantly affects regions with lower density and low star formation efficiency, resulting in unbound stellar groups.

1.1.3. Evolution of open clusters

After about 10 million years, the surviving clusters are free of their natal gas. However, these clusters do not orbit the Galactic center as bound systems forever. In addition to the high infant mortality rate in the first place, several further factors influence and shorten the lifetimes of these stellar systems. Oort et al. (1958) stated that there is a lack of old open clusters in the Milky Way. The reason for this is that open clusters suffer further disruption due to internal and external processes, and continuously lose mass. This mass loss destroys clusters, as they dissolve and evaporate stars into the field, which results in an enrichment of the Galactic field population.

In general, the dynamical evolution of a star cluster can be divided in two evolutionary stages (Martínez-Barbosa et al., 2016). The expansion-dominated phase is dominated by internal processes, whereas external forces dominate the evaporation-dominated phase. The expansion-dominated phase lasts for approx. 40% of a cluster's lifetime and is dominated by internal evolutionary effects. In this phase, open clusters lose mass due to stellar evolution and two-body relaxation, which results in an expansion of the open cluster's size. The main mechanisms of mass loss during the expansion-dominated phase are discussed in the following bullet points.

- Mass loss due to stellar evolution does not depend on the structure and orbit of the cluster (Lamers et al., 2010). Stars have different lifetimes, mainly depending on their mass. Stars with very high masses have the shortest lifetimes and generate mass loss in form of gas that is ejected (e.g. stellar winds, supernovae), already in the early stages of cluster evolution. Furthermore, their appearance changes into stellar remnants, such as white dwarfs, neutron stars or black holes.

- Additionally to stellar evolution, the so-called evolution-induced mass loss contributes to the dynamical evolution of star clusters. According to Lamers et al. (2010), this evolution-induced mass loss is due to the fact that the cluster radius expands and the tidal radius decreases during ongoing stellar evolution. This results in an escape of stars with velocities above the escape velocity. This mass loss is proportional to the mass loss by stellar evolution, but as it needs time to build up and does not start immediately, it amounts between 10-50% of the total amount of mass loss due to stellar evolution. Lamers et al. (2010)

- In addition to stellar evolution, star clusters lose mass due to two-body relaxation. According to Binney and Tremaine (1987), a star can escape a cluster by a single close encounter with another star. This produces a velocity change for both stars, and possibly one star reaches a velocity above the escape velocity. Also, more distant and therefore weaker encounters can gradually increase a star's energy, until an additional weak encounter is sufficient to give the star the necessary energy to escape. In addition to these effects, there exists equipartition, which is the tendency of kinetic energy to equalize during an encounter, and results in so-called mass segregation. This means that the more massive stars lose kinetic energy and sink towards the center, while lighter stars gain kinetic energy and their orbits expand, possibly until a star escapes the cluster (Binney and Tremaine, 1987).

In case the cluster has survived the expansion-dominated phase, the tidal effects of the Galaxy become important. This phase is called the evaporation-dominated phase (Martínez-Barbosa et al., 2016). In this stage, the cluster loses mass due to external effects (e.g. tidal stripping and interactions with spiral arms or giant molecular clouds), with the result that the cluster dissolves and stars dissipate into the field.

Tidal stripping is evoked because open clusters are situated in the disk region of the Galaxy and strongly influenced by the tidal field of the Milky Way. According to Kharchenko et al. (2009), the tidal forces of the Milky Way stretch clusters in ellipsoidal shaped oriented towards the Galactic center, and additionally produce cluster tails which pour out from the endpoints of the ellipsoids, known as so-called tidal tails. The reason for this is the differential rotation of our Galaxy. Disk galaxies like our Milky Way rotate differentially, thus follow a given rotation curve. In the solar neighborhood, all stars rotate with similar velocities. Stars closer to the Galactic center have higher angular velocities and overtake the cluster, forming a leading tail. Stars with larger galactocentric radii have lower angular velocities, and therefore lag behind the star cluster, building

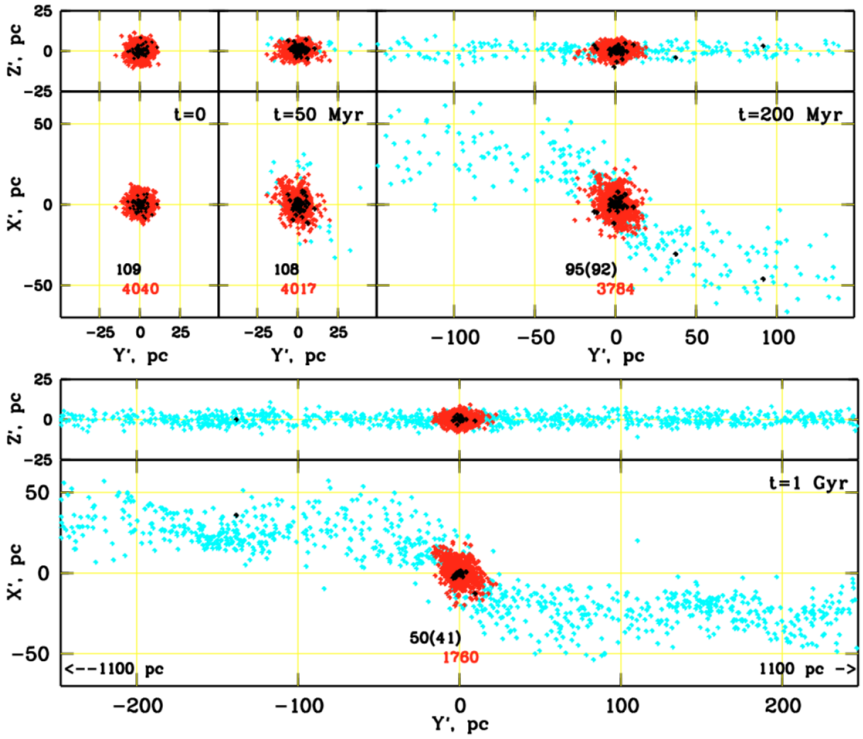

Figure 1.5.: The shape of a model cluster at different timesteps, unveiling the formation of tidal tails, as shown by N-body simulations. Credit: Kharchenko et al. (2009)

a trailing tail.

Figure 1.5 shows an N-body simulation done by Kharchenko et al. (2009). Their simulation shows that a spheroid model cluster with an initial mass $M_C = 10^3 M_\odot$ at a galactocentric distance $R_0 = 8.5$ kpc expands along the orbital path of the cluster over time. From top left to bottom right, the evolution of the cluster shape is illustrated for different timesteps. Clearly, there are no signatures of tidal tails during the first 50 Myr. However, after 200 Myr, the cluster already loses low-mass member stars at its ends farthest and nearest to the Galactic center, which results in the formation of more than 100 pc long tails of stars (cyan) escaping the cluster (red). For a cluster age of 1 Gyr, the tidal tails extend even over 1100 pc in both directions.

Chumak and Rastorguev (2006) studied the evolution of the middle-aged (600-700 Myr) open clusters Praesepe, Hyades, and Coma Berenices, as well as of the relatively young clusters ($<$ 120 Myr) Pleiades, α Persei, IC2391, and IC 2602. As can be seen in Figure 1.6, The older clusters reveal very prominent tidal tails, whereas the young clusters have not formed tidal tails yet. These tidal tail predictions were observationally confirmed by several recent studies. Meingast and Alves (2019) and Röser et al. (2019) revealed

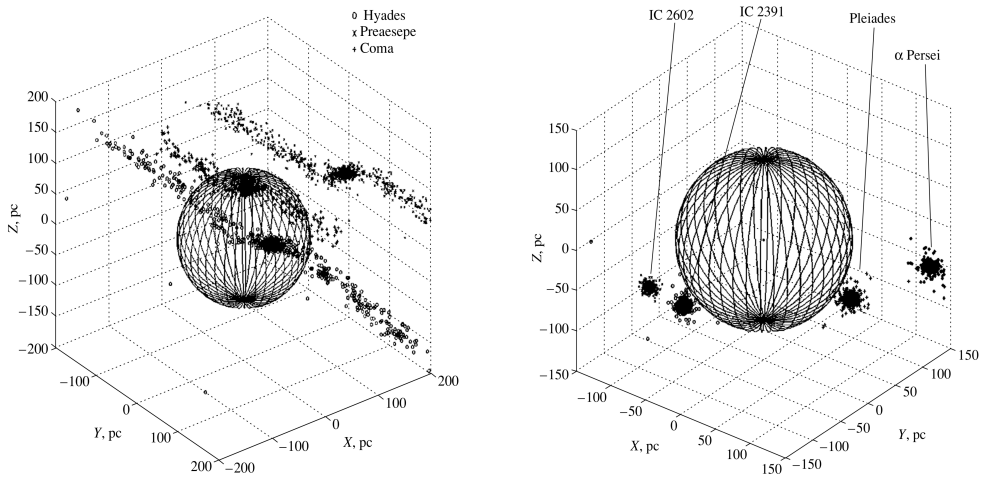

(a) Middle aged open clusters (600 - 700 Myr)

(b) Young open clusters ($<$ 120 Myr)

Figure 1.6.: N-body simulations for the evolution of open clusters in the solar neighborhood. Credit: O. Chumak and Rastorguev (2006)

the Hyades' tidal tails, Tang et al. (2019) and this work (Fürnkranz et al., 2019) showed the existence for Coma Berenices' tidal tails, and Röser and Schilbach (2019) unveiled the tidal tails which were predicted for Praesepe.

Additionally, interactions with the Galaxy's high-density regions, play an important role for the disruption of open clusters. Tidal shocks through the Galactic disk (disk shocks) or the Galactic bulge (bulge shocks), as well as passages through spiral arms and encounters with giant molecular clouds decrease the lifetime of star clusters significantly.

Martinez-Medina et al. (2017) performed a study on the evolution of high-altitude open clusters, investigating their mass loss as they witness strong tidal interactions while crossing the Galactic disk. Their study revealed that for star clusters up to 600 pc vertical orbital height, the lifetime decreases with increasing height. In this case, the crossing velocity is the main disruption factor. In the second case, for stars with an orbital height $>$ 600 pc, this trend is reversed, and from this point the lifetime of the cluster increases with increasing orbital height. In this case, the lifetime of a cluster is determined by the number of crosses through the disk, which decrease with increasing height (Martinez-Medina et al., 2017).

According to Boutloukos and Lamers (2003), the dissolution time t_{dis} of open clusters can be described with a power law depending on the initial mass of the cluster, which scales with the disruption time t_4 of a 10^4 $M_\odot$ cluster (see Equation 1.2). It shows

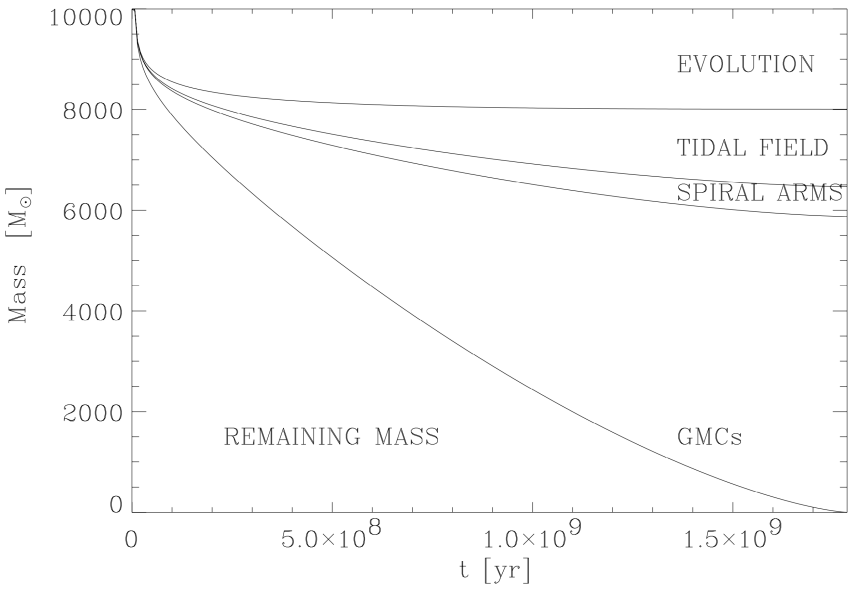

Figure 1.7.: Mass loss of an open cluster due to stellar evolution, tidal field, spiral arms, and giant molecular clouds. Clearly, giant molecular clouds are the main dissolution cause for open clusters. Credit: Lamers and Gieles (2006a)

that high mass clusters are expected to have longer lifetimes than clusters with lower mass. However, there appears to be a discrepancy between the observed dissolution times of open clusters in the solar neighborhood ($t_4 = 1.3$ Gyr for clusters with $10^2 < M < 10^4$, Lamers et al., 2005) and the disruption time found by N-body simulations ($t_4 = 6.9$ Gyr, Baumgardt and Makino, 2003). The fact that the observed disruption times are a factor 5 shorter is the result of external time-dependent perturbations (which have not been taken into account in these simulations), such as spiral arm passages and encounters with giant molecular clouds, which also affect the dissolution of open clusters significantly (Gieles et al., 2006).

$$t_{dis} = t_4 (M_i / 10^4 M_\odot)^{0.62} \tag{1.2}$$

Gieles et al. (2007) studied the effects of spiral arm passages, and Gieles et al. (2006) studied the effects of giant molecular clouds on the disruption of open clusters, respectively. Revealed by these studies, spiral arm passages contribute little to the disruption of open clusters, but giant molecular clouds turn out to be very dominant disruption factors in the evolution of open clusters. Lamers and Gieles (2006b) studied the evolution of open clusters with simulations taking into account stellar evolution, tidal stripping, shocking by spiral arms and encounters with giant molecular clouds. The mass loss of

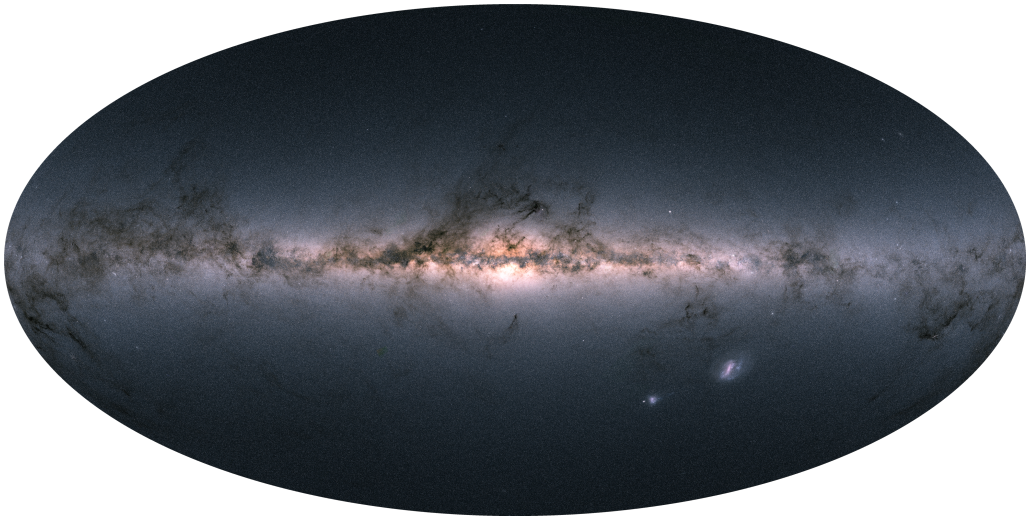

Figure 1.8.: This all-sky image of the Milky Way shows the brightness and colors of stars observed by *Gaia* DR2. Credit: ESA/Gaia/DPAC

a 10^4 $M_\odot$ open cluster due to these four separate effects is illustrated in Figure 1.7. It shows the mass loss of an open cluster as a function of time, and reveals that encounters with giant molecular clouds are the main dissolution effect of open clusters in the solar neighborhood. Moreover, these encounters and the subsequent large amount of mass loss can also explain the short observed dissolution rates for open clusters.

All those stars that leave their cluster of origin - be it from internal dynamical interactions or from external perturbations - live their existence as field stars until the end of their lives, and thus form our Galaxy's main stellar component.

1.2. Contribution of *Gaia*

The data provided by *Gaia* represent a unique opportunity to study the structure, formation and evolution of open clusters as discussed above. *Gaia* provides astrometric, photometric and spectroscopic measurements, full-sky coverage, has a very faint limiting magnitude, and delivers data with an accuracy and precision that was not available before.

Gaia is the follow-up mission of the first astrometric space mission Hipparcos, which operated between 1989 and 1993. *Gaia* was launched by the European Space Agency in 2013. Its launch vehicle was a Soyuz-Fregat rocket, which brought the satellite into a Lissajous-type orbit around the second Lagrange point. The science mission was designed to perform observations for five years, which has been extended until the end of 2020. Its primary goal is to measure positions, parallaxes and proper motions for one billion

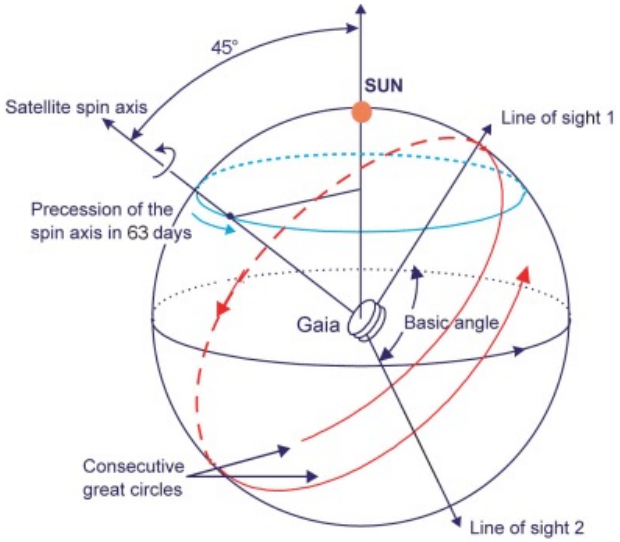

Figure 1.9.: An illustration of *Gaia*'s observation principle. Credit: ESA

stars, which corresponds to about one percent of the Galactic stellar population, with the aim to produce for the first time a 3D map of the Milky Way.

Figure 1.8 shows an all-sky view of our Galaxy as observed by *Gaia*. The colors are composed of the total amount of light with the blue and red light measured by *Gaia* in each pixel of the image. The flattened bright structure is the Galactic disk, in which most stars are located. The dark lanes across the plane are interstellar gas and dust, which cover the stars in their background. The two bright spots on the bottom left are the Small and Large Magellanic Clouds.

In order to map the stars in the Galaxy, the space observatory measures stars systematically in two field of views, which are separated by an angle of 106.5° (line of sight 1 and 2 in Figure 1.9). In order to observe a cycle, the spacecraft rotates 1° per minute (60 arcsec s^{-1}) around the satellite spin-axis, which is perpendicular to the field-of-views, so it scans a whole circle in six hours. Furthermore, the satellite's spin axis rotates in a 45° angle around the Sun (precession circle in blue in Figure 1.9). The resulting observed circles are illustrated in red in Figure 1.9.

On April 25, 2018, the second *Gaia* data release (*Gaia* DR2) was published. The catalogue contains data from 22 months of observation. It provides positions, parallaxes and proper motions (five-parameter astrometric solution) for more than 1.3 billion sources within limiting magnitudes of G = 21 mag and G = 3 mag, as well as radial velocity measurements for 7.2 million stars with G magnitudes between 13 mag and 4 mag. Furthermore, it delivers G magnitudes for more than 1.38 billion sources as well as BP/RP

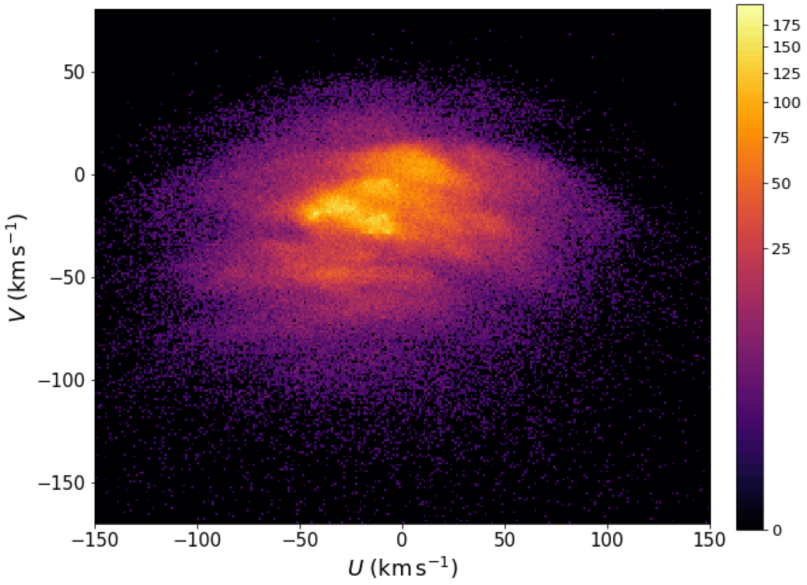

Figure 1.10.: Velocity plane of the stars in the solar neighborhood as measured by *Gaia*. The color scale indicates the number of stars per km s^{-1} bin. Credit: Gaia Collaboration et al. (2018b)

magnitudes for more than 1.38 billion stars, both with limiting magnitudes between G = 20 mag and G = 13 mag.

One of the first published results obtained with *Gaia* DR2 data is shown in Figure 1.10. It shows the velocity plane of stars in the solar neighborhood, and the color scale indicates the number of stars per km s^{-1} (Gaia Collaboration et al., 2018b). Already the first view shows that this parameter space is highly substructured, unveiling large, arch-like features that have not been seen in any data before. These large-scale structures are caused by resonances of the Galaxy's bar and spiral arms (Gaia Collaboration et al., 2018b). The most prominent arches (going from top to bottom) are the moving groups Sirius, Coma, Hyades and Pleiades, and the Hercules stream (which seems to be split into two branches). Moreover, a closer look at the velocity distribution enables smaller and more rounded structures on top of the large-scale structures. These small-scale velocity structures correspond to open clusters in the solar vicinity[3]. They are hardly visible in the velocity distribution, because the wealth of *Gaia* data superimposes these small velocity clumps, making their further investigation a challenging task.

[3]Unfortunately, the name 'moving group' is commonly in use for both the large-scale arch-like structures and the co-moving stellar associations in the solar neighborhood.

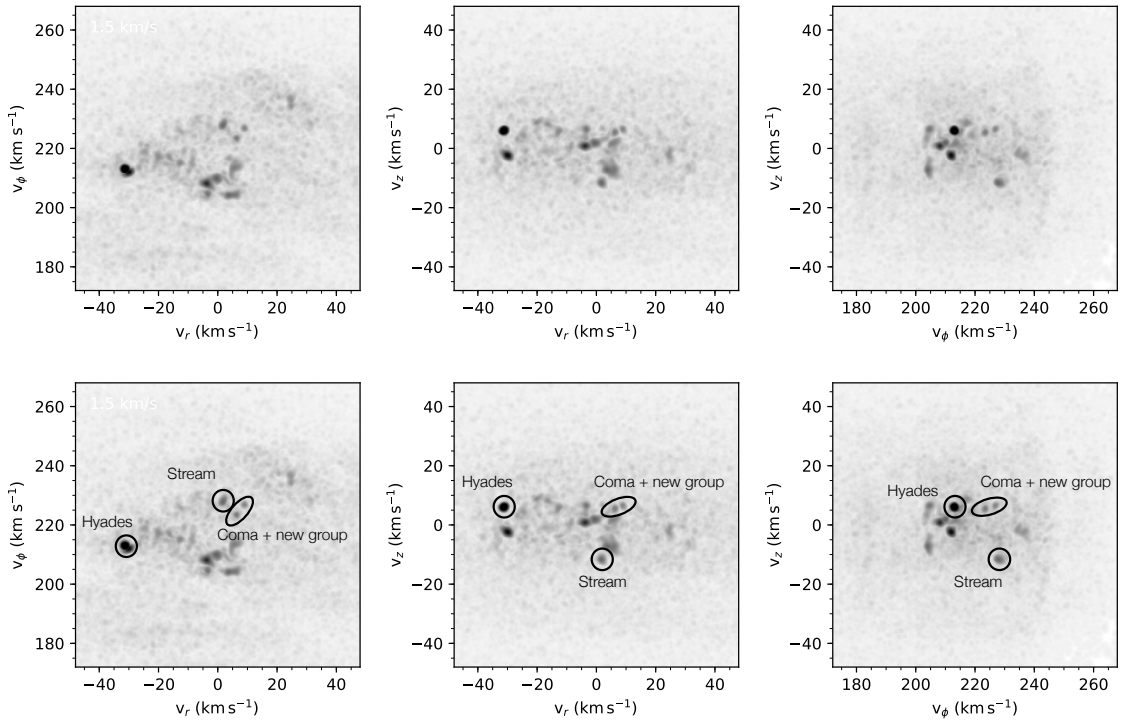

Figure 1.11.: Wavelet decomposition of stars in the solar neighborhood. Open clusters and associations are visible as small-scale overdensities. This work analyses the well-known cluster Coma Berenices at (v_r, v_ϕ) = (8.8 , 226.9) and a new moving group of stars at (v_r, v_ϕ) = (6.2 , 223.6). Credit: S. Meingast 2019

1.3. Motivation and goal of the thesis

Work done by Meingast et al. (2019) enables to extract these small-scale velocity structures from the *Gaia* DR2 velocity distribution. Figure 1.11 shows a wavelet decomposition of stars in the solar neighborhood. The selected velocity scale ranges from 1.5 to 3 km s^{-1} and allows open clusters to appear as prominent overdensities in the velocity distribution. The left panels of Figure 1.11 still show the arch-like structures as discussed in the previous section, but the small-scale overdensities, corresponding to open clusters, appear much more clearly.

This wavelet decomposition shows the small-scale velocity structure of the Milky Way disk in unprecedented detail, and was used as a starting point for the investigation of open clusters and associations in the solar neighborhood, and resulted in a paper series named "Extended stellar systems in the solar neighborhood". The studied stellar systems in this series are marked in the bottom panel of Figure 1.11. While the first paper revealed

long-expected tidal tails for the Hyades open cluster (Meingast and Alves, 2019), and the second paper reported the detection of a 120° stellar stream at a distance of only 100 pc (Meingast et al., 2019), this work analyses the well known star cluster Coma Berenices and a second previously unknown moving group of stars, both of which are visible as overdensities in the wavelet decomposition of stars in the solar neighborhood. These two groups do not only share very similar kinematics, they are also closely located in space. This unique configuration made us analyze the orbital motions of both groups in more detail, in order to predict a possible future open cluster encounter scenario. Such an incident has not yet been observed in our Galaxy before, therefore delivers new insights into our knowledge about the structure and dynamics of the Milky Way disk.

2. Methods description

This chapter describes the coordinate frames which were used for the investigation of Coma Berenices and its neighbor moving group, explains the astrometric position and velocity data provided by *Gaia* DR2, and shows the calculation of additional coordinates and velocities. Moreover, it provides a description of the orbit integration done for both groups and discusses the uncertainties and errors of orbital parameters in this context. Last, it explains the clustering method which was used to obtain a meaningful membership determination for both groups and describes our approach to estimate the contamination fraction.

2.1. Calculation of galactic coordinates and velocities

The *Gaia* catalogue contains the position angles of the equatorial coordinate frame (spherical) in right ascension (α) and declination (δ) in degrees. The coordinates are given in the International Celestial Reference Frame (ICRF), and origin at the barycenter of the Solar System. Its main advantage is that the axes are fixed and do not depend on the motion of Earth. Additional spherical coordinates, namely galactic longitude (l) and galactic latitude (b) are also provided by *Gaia*. This coordinate system is a simple rotation of the equatorial system and more convenient for studying the Galaxy. This coordinate frame origins at the position of the Sun. The longitude measures the angular distance along the Galactic equator, and the latitude represents the angle north our south of the Galactic plane.

In addition, the *Gaia* catalogue provides parallax measurements. The parallax (ϖ) is defined as the angle between two lines of sight, which observe the same object from two different locations. It is used as a distance (d) indicator for stars. As Earth rotates around the Sun, the positions of the stars seem to move, where the movements of the closer stars seem to be larger. Therefore, the parallax can be described as an apparent shift of the stars. The connection between parallax and distance of a star is given by the following relation:

$$d = \frac{1}{\varpi} \tag{2.1}$$

Here, the distance is given in units of parsec and the parallax in arcseconds. However, for this work, a more advanced bayesian distance estimate by Bailer-Jones et al. (2018)

was used, as it accounts for the non-linearity of the transformation between parallax and distance.

In addition to coordinates, *Gaia* also observes the motions of the stars, in particular the radial velocity and proper motions. The radial velocity (*rv*) in km s^{-1}, or line-of-sight-velocity shows how fast a star moves towards or away from us. The proper motions of a star represent its apparent change in the on-sky position compared to the background. They are given in equatorial coordinates, namely μ_α and μ_δ, and have units of mas yr^{-1} in the *Gaia* catalogue. The published proper motion in right ascension is $\mu_\alpha = \mu_\alpha \cdot cos(\delta)$. The proper motions can be transformed from equatorial coordinates to galactic coordinates, resulting in μ_l for the longitude and μ_b for the latitude. In contrast to *rv*, proper motions are dependent on the distance, as more distant stars have smaller proper motions. Furthermore, proper motions together with the distance can be used to derive the tangential/transverse velocities of a star, because this motion cannot be measured directly. The conversion from proper motions to tangential velocities is given by the following equation:

$$v_t = 4.74 \cdot \mu \cdot d \tag{2.2}$$

Here, the tangential velocity is given in km s^{-1}, the proper motion in mas yr^{-1}, and the distance in units of parsec. Using this equation, we obtain tangential velocities v_α and v_δ for the equatorial system, and v_l and v_b in galactic coordinates.

We can use the data provided by *Gaia* to calculate galactic cartesian coordinates and velocities. The galactic cartesian coordinate frame is centered at the Sun and is described with the coordinates X, Y and Z in parsec. X is pointing towards the Galactic center, Y is positive in the direction of Galactic rotation, and Z is positive towards the north Galactic pole. We obtain these coordinates by calculating them with the following equations:

$$\begin{aligned} X &= d \cdot cos(l) \cdot cos(b) \\ Y &= d \cdot sin(l) \cdot cos(b) \\ Z &= d \cdot sin(b) \end{aligned} \tag{2.3}$$

In order to calculate the corresponding velocities, we additionally need the radial velocity and the tangential velocities in galactic coordinates. The velocities U, V and W in km s^{-1} can then be calculated according to the following equations (e.g. Bobylev and Bajkova, 2019):

$$
\begin{aligned}
U &= rv \cdot cos(l) \cdot cos(b) - v_l \cdot sin(l) - v_b \cdot cos(l) \cdot sin(b) \\
V &= rv \cdot sin(l) \cdot cos(b) + v_l \cdot cos(l) - v_b \cdot sin(l) \cdot sin(b) \\
W &= rv \cdot sin(b) + v_b \cdot cos(b)
\end{aligned} \tag{2.4}
$$

These velocities can also be corrected with the local standard of rest. The local standard of rest represents the mean motion of stars in the neighborhood of the Sun (assuming they move around the center of the Galaxy in a perfectly circular orbit). Therefore, we can use the convention by Schönrich et al. (2010) to calculate the corrected velocities:

$$
\begin{aligned}
U_{LSR} &= U + 11.1\ kms^{-1} \\
V_{LSR} &= V + 12.24\ kms^{-1} \\
W_{LSR} &= W + 7.25\ kms^{-1}
\end{aligned} \tag{2.5}
$$

If we study the Milky Way on global scale, it is more convenient to use a galactocentric coordinate frame, which is centered at the Galactic center. In order to adopt this coordinate frame, we have to add additional information. We assume that the Sun is located at a distance of $R_0 = 8300$ pc away from the Galactic center (Gillessen et al., 2009), at a height of 27 pc above the plane Chen et al. (2001). Also, the circular velocity at R_0 is assumed to be 220 km s^{-1} (Kerr and Lynden-Bell, 1986). As we are dealing with motions of stars (which are approximately circular), it is more convenient to use a cylindrical coordinate frame instead of a cartesian coordinate frame. Using a simple coordinate transformation, we can transform the cartesian coordinates into cylindrical coordinates. First, we have to calculate the position angle Θ with the following relation:

$$
tan(\Theta) = \frac{Y}{(R_0 - X)} \tag{2.6}
$$

This angle can then be used to calculate the galactocentric cylindrical velocities in km s^{-1}:

$$
\begin{aligned}
v_r &= -U \cdot cos(\Theta) + (V_0 + V) \cdot sin(\Theta) \\
v_\phi &= U \cdot sin(\Theta) + (V_0 + V) \cdot cos(\Theta) \\
v_z &= W_{LSR}
\end{aligned} \tag{2.7}
$$

A comparison between the galactic cartesian velocities and the galactocentric cylindrical

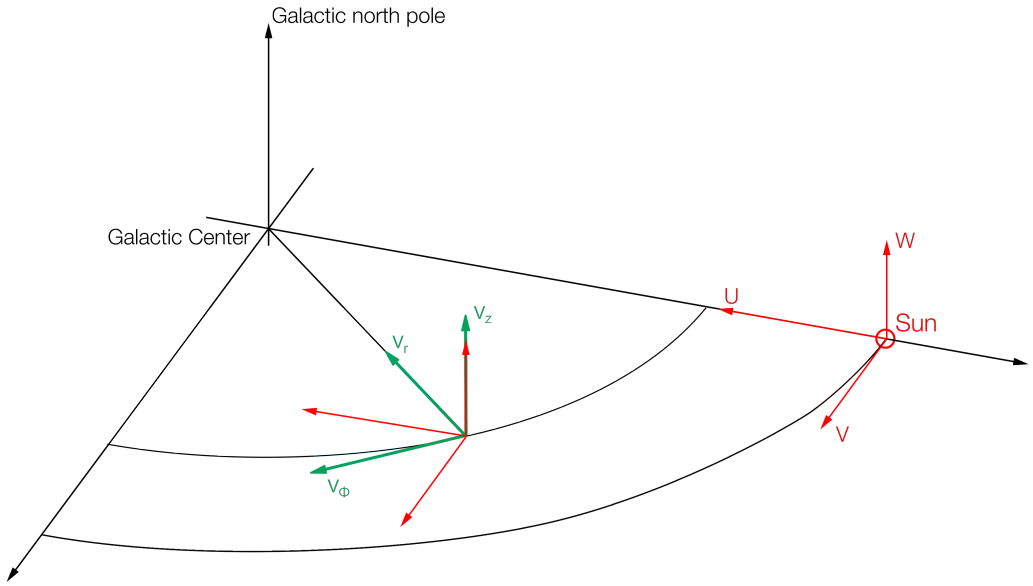

Figure 2.1.: Comparison between galactic cartesian velocities UVW (red) and galactocentric cylindrical velocities (green). Credit: S. Meingast 2019

velocities can be seen in Figure 2.1. Independent of the location in the Galaxy, the UVW velocity vectors (red) are always oriented with respect to the Sun's current position. In contrast, the $v_r v_\phi v_z$ velocity vectors (green) are always oriented with respect to the Galactic center. In other words, while galactic cartesian coordinates are static, the galactocentric cylindrical coordinate system is corotating, which is a main advantage when investigating the dynamics of a rotating system like the Milky Way.

2.2. Galactic dynamics

Our investigation of Coma Berenices and its neighbor group contains a very detailed kinematic analysis. Although both groups show a generally very similar kinematic profile, we do find relevant differences between both groups when examining the galactocentric cylindrical velocities. Figure 2.2 shows the YZ view of all stars with radial velocity measurements, color-coded in v_r, v_ϕ, and v_z (left to right). As revealed by Figure 2.2, there is a clearly visible difference between the radial and azimuthal velocity components of both groups ($\Delta v_r = 2.9$ km s^{-1}, $\Delta v_\phi = 3.5$ km s^{-1}), whereas the vertical velocity component is virtually identical. I addition to the more than 3 km s^{-1} higher velocity of Coma Berenices in the direction of rotation, Coma Berenices is lagging behind its neighbor group in this direction. This configuration can clearly be seen in the middle

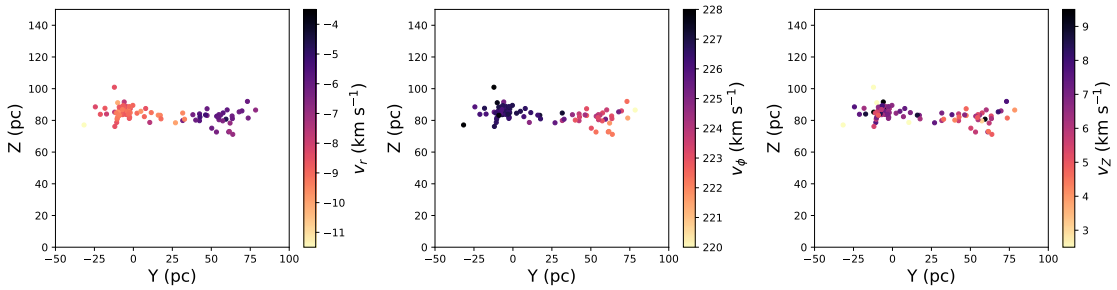

Figure 2.2.: YZ view of Coma Berenices and its neighbor group, color-coded in galactocentric cylindrical velocities v_r, v_ϕ, and v_z (left to right).

panel of Figure 2.2, and indicates a potential drift of Coma Berenices into its neighbor group within the near future. In order to investigate this plausible encounter scenario, we perform an orbit integration of both groups, and provide a detailed description of orbit initialization and error calculation below.

2.2.1. Orbit integration with Galpy

In order to calculate the orbits of Coma Berenices and its neighbor group, we use Galpy, which is a Python package for galactic dynamics (Bovy, 2015), and provides a number of galactic potentials. We use the recommended MWPotential2014 (Bovy, 2015), which includes a bulge, a disk and a dark-matter halo. However, it is a very basic model of the Milky Way potential, and therefore does not include non-axisymmetric components, like spiral arms or a bar.

We initialize the orbits with the following observational *Gaia* DR2 data: the position in right ascension and declination, the distance, the proper motions in right ascension and declination, and the radial velocity. In addition to this, the following assumptions complete the initialization: the galactocentric distance of the Sun $r_0 = 8.3$ kpc, the height of the Sun above the plane $z_0 = 27$ pc, the circular velocity of the Sun $v_0 = 220$ km s^{-1}, and the Solar motion (11.1, 12.24, 7.25) km s^{-1}, which was taken from Schönrich et al. (2010).

Figure 2.3 illustrates the movement of an open cluster in the Milky Way. Particularly, it shows the orbit of Coma Berenices, integrated backwards for 700 Myr, the approximate time of its birth. The track of the cluster is shown in blue, and the Galactic center (GC) is marked with a black dot. It is important to note that Figure 2.3 represents an 'ideal', and therefore unrealistic scenario, as in this setup the open cluster does not suffer any perturbations during 700 Myr. In reality, interactions between the cluster and the galactic plane, encounters with spiral arms or giant molecular clouds, dynamical

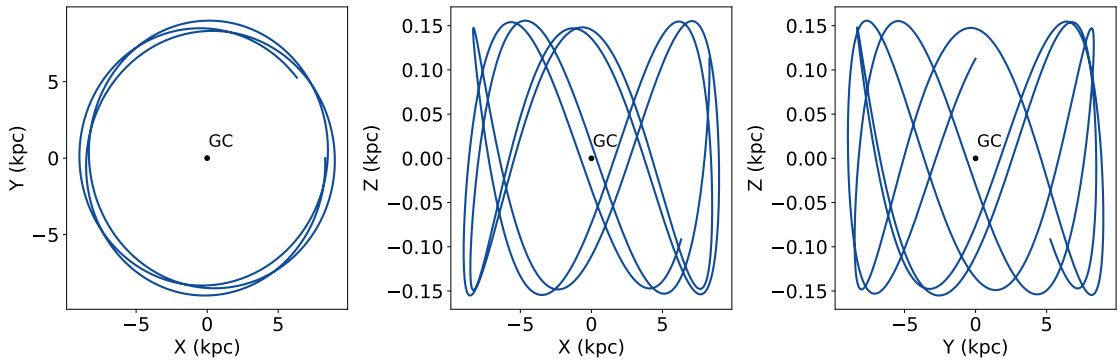

Figure 2.3.: Orbit of Coma Berenices, integrated using Galpy backwards for 700 Myr, the approximate time of its birth.

friction and further perturbations influence the movement of an open cluster. However, the top-down view in the left panel shows that - in an unperturbed case - typical open clusters orbit the Galactic center on nearly circular tracks. In addition to this, the middle and right panel unveil an up- and down movement of the open cluster perpendicular to the Galactic plane. In the example case of Coma Berenices, the largest distance to the galactic plane is 150 pc in both directions. After reaching this maximum, the cluster starts to move towards the plane again. Furthermore, we see that during its lifetime, Coma Berenices has circled the Galactic center and passed the Galactic plane several times already.

2.2.2. Uncertainties and errors of orbital parameters

The observational data we use to initialize the orbits have errors in measurement. Due to this fact, a forward or backward integration becomes inaccurate, and we have to calculate the uncertainty of the orbital parameters due to these measurement errors, in order to provide proper information about the movement of Coma Berenices and its neighbor group. We perform the orbital uncertainty calculation in three steps, which are described in detail below.

First, we sample the initial parameters of each star from the error distribution, in order to obtain a meaningful prediction of the uncertainties of orbit integration. To do so, we make the assumption that the errors in measurement are symmetric, and use a normal distribution for the errors, with the actual measurement as mean and the standard deviation as error. The method to compute uncertainties was adopted from Price-Whelan (2017).

Due to the very precise position measurements, we do not sample in right ascension and

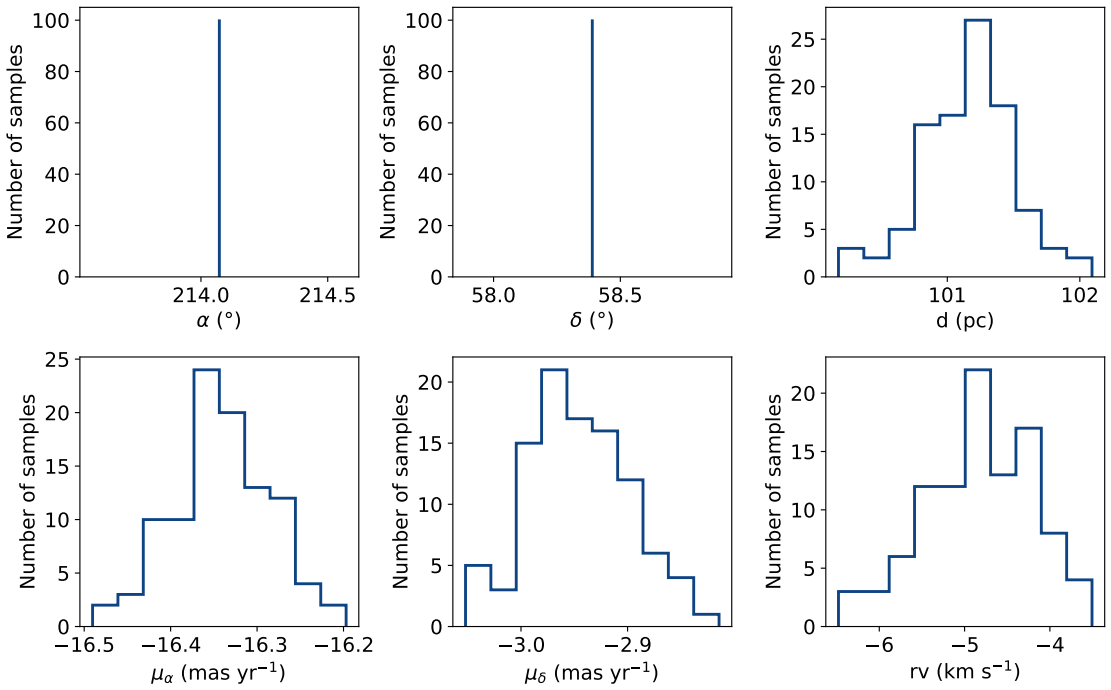

Figure 2.4.: Distribution of the orbital parameters for one example star after sampling from the error distribution.

declination. The errors - namely the standard deviation - for proper motions and radial velocity were provided by the *Gaia* catalogue. In order to obtain the error in distance, we use the following equation, where the distance is given in units of parsec, and the parallax is given in mas:

$$\delta d = 1000 \cdot \frac{\delta \varpi}{\varpi^2} \tag{2.8}$$

Figure 2.4 shows the distribution of the orbital parameters for one example member star in Coma Berenices, after sampling from the error distribution. The first two panels show right ascension and declination, which we did not sample. The other orbital parameters show normal distributions. Looking at the sampling distributions reveals that $3\sigma \sim 0.1$ mas yr^{-1} for proper motions, $3\sigma \sim 0.7$ pc for distance, and $3\sigma \sim 1.6$ km s^{-1} for radial velocity. The large distribution of radial velocities results from the large measurements errors of the observational radial velocity data.

Second, we integrate the orbit for every sampling for every star for every timestep for the next 50 Myr. Third, we calculate the orbital uncertainty in two different ways. In order to obtain the uncertainties of the distance between both groups in the future,

we calculate for every sampling for every timestep the XYZ coordinates of the cluster centers, which is done by calculating the mean XYZ value for each group. We then calculate for every sampling for every timestep the distance between the cluster centers, and extract for every timestep the mean value, as well as the standard deviation (3σ). In order to get the uncertainties of the XYZ positions of every single star in the future, we calculate for every timestep for every star the mean value and the standard deviation (3σ).

2.3. Cluster membership determination

In order to study open clusters, it is essential to identify their member stars. This section explains the methods we use to distinguish cluster member stars from field stars and describes our approach to estimate the contamination fraction of our member selection.

2.3.1. Clustering with DBSCAN and k-NN algorithm

Stars of an open cluster were born and move together (Castro-Ginard et al., 2019). This implies that stars of open clusters are likely to share the same velocity and galactic volume. Considering this fact, we select cluster member stars in two steps, which are discussed in more detail below, but briefly summarized here: Firstly, we associate clusters with overdensities in velocity space. In particular, we apply the density-based clustering algorithm DBSCAN (Ester et al., 1996) on 2D tangential velocities (v_α, v_δ), and extract stars located in overdensity spots. Secondly, we apply the k-NN algorithm to sort out sources which are spatially not connected to the clusters. Following this membership determination, we find that the extracted sources follow narrow and well-defined main sequences on a Hertzsprung-Russel diagram, proving that our method selects open cluster member stars properly, as each sequence represents a coeval stellar population.

There are a variety of clustering algorithms which are able to identify similar objects in a data set, and group them into clusters. In order to cluster stars with similar velocities, we chose the density-based algorithm DBSCAN (Ester et al., 1996). It has the ability to discover clusters with arbitrary shape, and additionally, it can identify outliers (noise points). Both features are essential for this work, as both groups do not appear as perfect point-like structures in velocity space, and as we do not want to cluster probable field stars. In addition, DBSCAN requires two parameters, namely the cluster size *MinPts* and the linking length ϵ, which are easy to tune in a physically reasonable way. MinPts represents the minimum number of points to form a dense region, and ϵ represents the radius of the sphere around a point. The principle of the clustering algorithm is illustrated

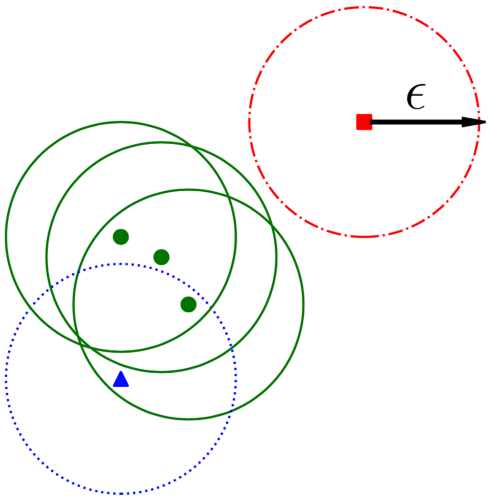

Figure 2.5.: Ann illustration of the DBSCAN method. Core points are colored in green, neighbor points are represented in blue, and noise points are illustrated in red. Credit: Castro-Ginard et al. (2018a)

in Figure 2.5. The algorithm differs between three kinds of points: core points (green), neighbor points (blue) and noise points (red). A core point is defined as a point that has *MinPts* neighbors within its radius ϵ. Neighbor points are points that are within the ϵ radius of a core sample, but are not a core sample themselves. Core points and neighbor points are all part of a cluster. A noise point is a point that is not within the radius ϵ of a core point, and therefore not part of the cluster. Figure 2.5 shows the example case of $MinPts = 3$ (the length of ϵ is illustrated with an arrow).

Figure 2.6 illustrates the behavior of the two parameters *MinPts* and ϵ. Each panel shows the tangential velocity space around the velocity coordinates of Coma Berenices and its neighbor group. The linking length ϵ rises from left to right in 0.1 km s^{-1} steps, and the cluster size *MinPts* increases from top to bottom in 10-point steps. The performance plots reveal that if ϵ is too small, a large part of the data will not be clustered (left column). On the other hand, if ϵ is too high, clusters will start to merge (right column). Looking at the behaviour of *MinPts*, we find that larger values form more compact clusters (going from top row to bottom row). However, too compact clusters tend to loose stars which should be associated with the clusters. The panel in the center ($MinPts = 70$, $\epsilon = 0.5$ km s^{-1}) shows our final parameter setup. This setup was chosen, because it delivers two pronounced velocity clusters associated with the two prominent overdensities in velocity space and assigns both clusters a high number of probably member stars.

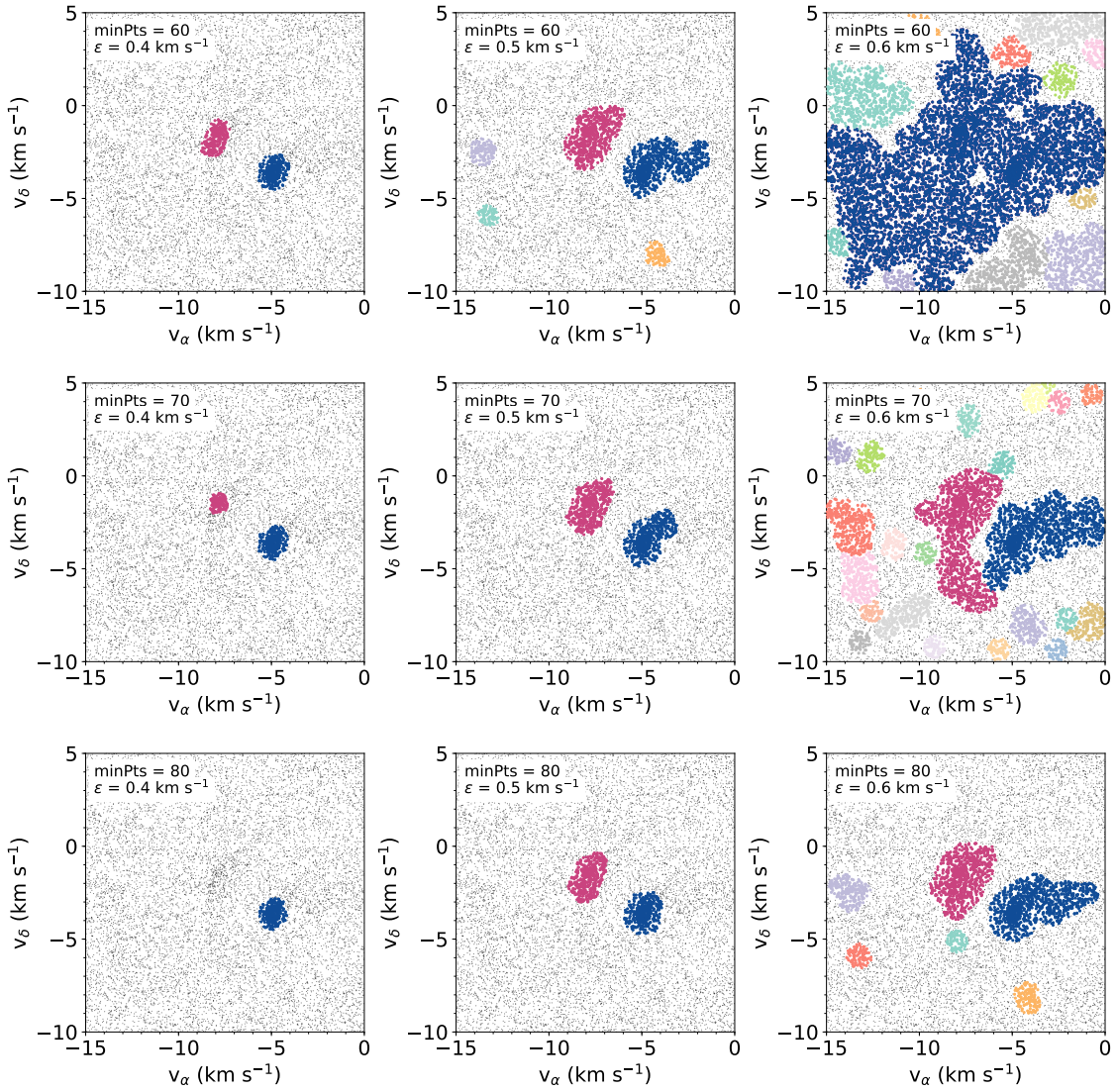

Figure 2.6.: Performance of DBSCAN for a varying set of parameters. The linking length ϵ rises from left to right in 0.1 km s^{-1} steps, and the cluster size *MinPts* increases from top to bottom in 10-point steps.

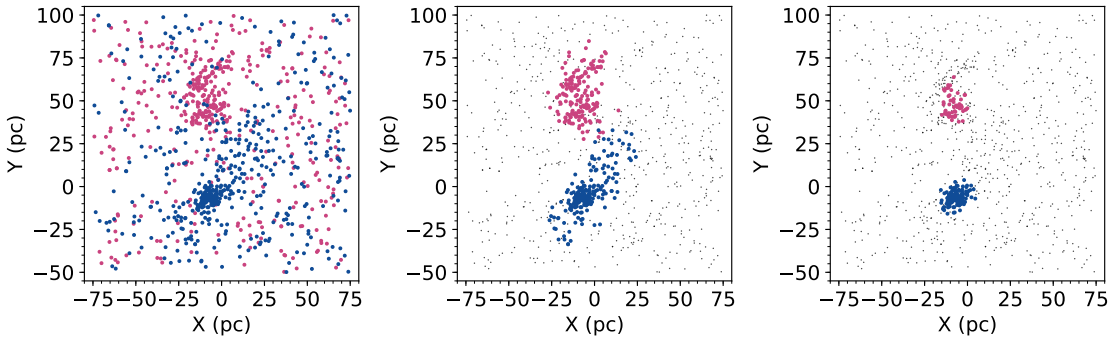

Figure 2.7.: Top down view on Coma Berenices and its neighbor group. Illustrated is the member selection after no spatial filtering (left), and after applying the final nearest neighbor criterium that excludes all stars with less than 30 neighbors within 20 pc (middle), in comparison with a too conservative (40 neighbors within 10 pc) filter (right).

In addition to the clustering in tangential velocities, we assume that member stars of both groups must also be grouped in spatial coordinates. Therefore, we apply a spatial density filter on our velocity selection, in order to clean our member selection. We use the simple classification algorithm k-NN (k-nearest neighbor), which assumes that similar objects in a data set are near each other. The algorithm computes the Euclidean distance of every point of one cluster to k other points of the same cluster. We then sort out stars which do not spatially connect with the clusters by excluding stars which do not have a certain number of neighbors within a defined distance of the star.

Figure 2.7 illustrates the effect of applying a k-nearest neighbor criterion. All panels show Coma Berenices and its neighbor group in galactic cartesian coordinates. The left plot displays the member selection of both groups after DBSCAN clustering without applying a spatial density filter. Although both clusters are clearly visible, a large fraction of stars appear to be randomly scattered in space, indicating that they do not belong to one of the clusters. This shows the need of an additional spatial filtering, as clustering in velocities alone is not sufficient enough. The middle panel shows the final filtering criterion that excludes all stars with less than 30 neighbors within 20 pc. This setup perfectly unveils the structure of both clusters, with all stars remaining that physically belong to the clusters. In order to show how important a well-chosen filter is, the right panel of Figure 2.7 illustrates a very conservative criterion, excluding all sources with less than 40 neighbors within 10 pc. In this setup, only the stars in the central parts

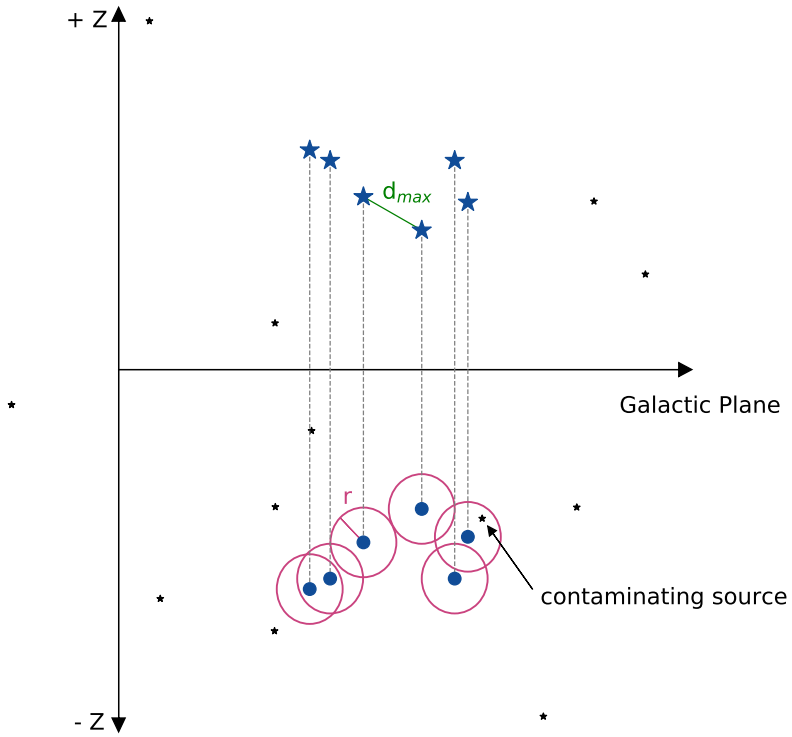

Figure 2.8.: 2D Illustration of the contamination estimate approach, which represents the spacial components of the estimate.

of both clusters remain, which leads to a loss of a large fraction of potential members stars.

2.3.2. Contamination fraction estimate

As described above, we carefully select candidate member stars for Coma Berenices and its neighbor group. However, it is very likely that our selection still contains sources which do not belong to one of the groups. We therefore estimate the contamination fraction of our selection by extracting sources in a symmetric phase-space on the opposite side of the Galactic plane (see also Meingast et al., 2019). This is performed in three steps which are described below. A 2D illustration of the approach is shown in Figure 2.8.

First, we invert the vertical velocity component (v_z) of the cluster members. Next, we take the whole *Gaia* database and apply the error cuts which were used throughout this work. We extract all stars (with radial velocity measurements) that have velocities

within 3σ of the velocity dispersion of the clusters. Second, we mirror all group sources around the Galactic plane. We do this by simply inverting the Z-coordinates of the stars. Third, we make a sphere around each mirrored star. The radius of the sphere is half the maximum nearest neighbor distance of the group member stars. To obtain the contamination fraction, we count the *Gaia* database stars which are located within one of the spheres. The number of these stars represents the contamination fraction of our member selection.

Figure 2.8 represents a simple 2D illustration of the contamination estimate. The blue stars represent member stars of a cluster. The maximal nearest neighbor distance between two stars is d_{max}. All stars are mirrored into the opposite side of the Galactic plane, and their mirrored counterparts are illustrated with blue dots. The small black dots represent stars that were selected from the *Gaia* database, and have velocities within 3-σ of the velocity coordinates of the group (with inverted v_z). The magenta spheres around the mirrored stars have a radius of $d_{max}/2$. In the example illustration of Figure 2.8, one *Gaia* database star is located within a sphere, from what follows that we have one contaminating source in this case.

3.Coma Berenices and its neighbor moving group

3.1. Overview

This article is the third part of our paper series "Extended stellar systems in the solar neighborhood", in which we study the structure, dynamics, and evolution of open clusters and associations in the solar neighborhood. It is the result of our investigations of Coma Berenices and a second moving group of stars in its velocity and spatial neighborhood. We find that both groups will share the same Galactic volume in 13 Myr. This cohabitation is temporal, as both groups are not massive enough for merging to occur. We estimate that such encounter events are not rare in the Milky Way, but can happen about once per Galactic revolution for each cluster.

3.2. Publication details

Title: Extended stellar systems in the solar neighborhood: III. Like ships that pass in the night: the Coma Berenices neighbor moving group
Authors: Verena Fürnkranz, Stefan Meingast, and João Alves
Section: Letters to the Editor
Status: Accepted for publication in Astronomy & Astrophysics
Date of acceptance: March 12, 2019
Publication date: April 16, 2019
Bibliographic reference: A&A 624, L11 (2019)
DOI: 10.1051/0004-6361/201935293
Online data: http://cdsarc.u-strasbg.fr/viz-bin/qcat?J/A+A/624/L11
Own contributions: Literature research, *Gaia* data analysis and interpretation, Plots and Figures, Paper writing

A&A 624, L11 (2019)
https://doi.org/10.1051/0004-6361/201935293

Astronomy & Astrophysics

LETTER TO THE EDITOR

Extended stellar systems in the solar neighborhood

III. Like ships in the night: the Coma Berenices neighbor moving group*

Verena Fürnkranz[1], Stefan Meingast[1], and João Alves[1,2,3]

[1] Department of Astrophysics, University of Vienna, Türkenschanzstrasse 17, 1180 Wien, Austria
e-mail: verena.fuernkranz@univie.ac.at
[2] Radcliffe Institute for Advanced Study, Harvard University, 10 Garden Street, Cambridge, MA 02138, USA
[3] Data Science at Uni Vienna, Faculty of Earth Sciences Geography and Astronomy, University of Vienna, Austria

Received 18 February 2019 / Accepted 12 March 2019

ABSTRACT

We report the discovery of a kinematically cold group of stars, located in the immediate neighborhood of the well-known star cluster Coma Berenices (Mel 111). The new group identified in tangential velocity space as measured by *Gaia* contains at least 177 coeval members distributed in two subgroups, and appears as a flattened structure parallel to the plane, stretching for about 50 pc. More remarkably, the new group, which appears to have formed about 300 Myr later than Mel 111 in a different part of the Galaxy, will share essentially the same volume with the older cluster when the centers of both groups will be at their closest in 13 Myr. This will result in the mixing of two unrelated populations with different metallicities. The phase of cohabitation for these two groups is about 20–30 Myr, after which the two populations will drift apart. We estimate that temporal cohabitation of such populations is not a rare event in the disk of the Milky Way, and of the order of once per Galactic revolution. Our study also unveils the tidal tails of the Mel 111 cluster.

Key words. stars: kinematics and dynamics – solar neighborhood – open clusters and associations: individual: Coma Berenices

1. Introduction

Stellar clusters are unique probes of the physical and chemical conditions at their time and place of birth in the Galaxy. *Gaia* provides reliable distances and kinematics to a large number of cluster members and with an unprecedented accuracy. This is causing a renewed interest in the field, in particular in validating ideas for which observational data was lacking. For example, long-suspected dynamical features such as tidal tails have now been identified for the nearest cluster to Earth, the Hyades cluster (Röser et al. 2019; Meingast & Alves 2019; hereinafter Paper I). At the same time, the expected counterparts of old disk clusters and associations are now beginning to be unveiled (Ibata et al. 2019; Meingast et al. 2019; hereinafter Paper II). This newly available parameter space promises to open a new window on cluster disruption, the build up of the field population, the quantification of anisotropies in the mass distribution of the Milky Way disk, and the homogenization of different stellar populations.

Nevertheless, there is room for surprises. In this Letter we present our follow-up work on the "Extended stellar systems in the solar neighborhood" series. While a final catalog is in preparation (Meingast et al., in prep.), we report here evidence for temporal cohabitation of different stellar populations in the same Galactic volume. The clusters in question, Coma Berenices (Mel 111) and a newly found moving group in the velocity and spatial neighborhood, are not massive enough for capture of populations to occur, but they will appear in the near future, and for a limited time, as a multi-population cluster.

2. Data description and member selection

As in Paper II, we detected overdensities in velocity space, given by *Gaia* DR2 (Gaia Collaboration 2016, 2018b), with a wavelet decomposition in Galactocentric Cylindrical coordinates[1]. Among the extracted significant peaks, we found the velocity coordinates of the well-known star cluster Mel 111 at $(v_r, v_\phi, v_z) = (8.83, 226.93, 6.54)\,\mathrm{km\,s^{-1}}$, as well as a nearby second overdensity at $(v_r, v_\phi, v_z) = (6.21, 223.57, 5.41)\,\mathrm{km\,s^{-1}}$, belonging to a previously unknown stellar population. An extraction of all sources within a $5\,\mathrm{km\,s^{-1}}$ radius around the identified peaks indicated that both populations do not only share very similar velocities, but are also adjacent in spatial coordinates, making them an interesting case for further investigation on possible cluster interactions.

In order to minimize the error budget, we adopted filtering criteria similar to Paper II: $\sigma_{\mu_{\alpha,\delta}}/\mu_{\alpha,\delta} < 0.5$, $\sigma_\varpi/\varpi < 0.5$, and $\max_{\sigma 5D} < 0.5$. Since Mel 111 and its newly discovered neighbor are located well above the Galactic plane, we also restricted our database to $0\,\mathrm{pc} < Z < 150\,\mathrm{pc}$, $-75\,\mathrm{pc} < X < 75\,\mathrm{pc}$, and $-50\,\mathrm{pc} < Y < 100\,\mathrm{pc}$.

In contrast to the prominent stream identified in Paper II, here we find structures with smaller spatial extent. In such cases

* Full Table A.2 is only available at the CDS via anonymous ftp to cdsarc.u-strasbg.fr (130.79.128.5) or via http://cdsarc.u-strasbg.fr/viz-bin/qcat?J/A+A/624/L11

[1] For details on the coordinate system definition see Paper I.

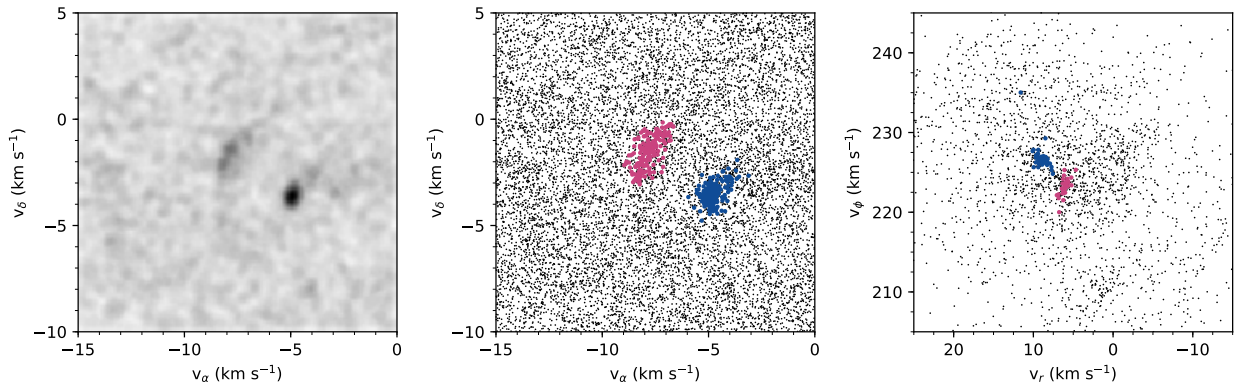

Fig. 1. *Left panel*: KDE, using an Epanechnikov kernel with a bandwidth of 0.4 km s^{-1} in the tangential velocity space for the 11 294 stars in our final database. Two prominent overdensities are visible, corresponding to Mel 111 and the new group which are displayed in the middle panel in blue and magenta, respectively. *Right panel*: our selection in the $v_r v_\phi$–velocity plane. Small black dots represent all sources from the filtered *Gaia* database.

projection effects are minimized and consequently we based our member selection on 2D tangential velocity space (v_α, v_δ) rather than on 3D velocities. We obtained tangential velocities for every source from proper motion and distance data, and applied a further restriction of $-15\,\mathrm{km\,s^{-1}} < v_\alpha < 0\,\mathrm{km\,s^{-1}}$ and $-10\,\mathrm{km\,s^{-1}} < v_\delta < 5\,\mathrm{km\,s^{-1}}$. After applying these filters, a total number of 11 294 sources remained. The tangential velocity distribution of the remaining sources is illustrated with a kernel density map in the left panel of Fig. 1. In this view, two local overdensities become clearly visible. The tight, point-like structure at $(v_\alpha, v_\delta) \sim (-5, -4)\,\mathrm{km\,s^{-1}}$ contains sources associated with Mel 111, whereas the elongated arc-shape at $(v_\alpha, v_\delta) \sim (-8, -2)\,\mathrm{km\,s^{-1}}$ represents a previously unknown stellar group.

Following the setup outlined above, we then extracted clustered sources with the density-based algorithm DBSCAN (Ester et al. 1996). Specifically for our selection, we manually chose minPts = 70, $\epsilon = 0.5\,\mathrm{km\,s^{-1}}$ for the DBSCAN setup which resulted in two tangential velocity clusters associated with the two apparent overdensities in the left panel of Fig. 1. This selection extracted 245 sources of Mel 111, and 237 stars associated with the new group. Following the previous papers, we additionally restricted the selection by applying a spatial density filter. We tested several setups, where our final criterion excludes all sources that have less than 30 neighbors within 20 pc. Finally, we manually removed one star that was located below the main sequence and also showed a large photometric excess factor, indicating contaminated *Gaia* photometry. This resulted in a final selection of 214 Mel 111 sources and 177 sources for the new group. Table A.1 lists several parameters measured for these two groups.

The middle panel of Fig. 1 shows the final selection for both groups in the tangential velocity space. While the blue points represent our member selection for Mel 111, the new group is illustrated in magenta. For clarity, these colors are the same for all the figures presented here. The right panel of Fig. 1 displays the distribution of the stars in the $v_r v_\phi$–velocity plane, where the two significant overdensities are colored corresponding to our member selection of Mel 111 and the new group. It shows both populations tightly clustered, thus verifying our selection process.

We estimated the contamination level with two methods. First, we applied the same method as described in Paper II, which extracts sources in a symmetric phase-space region on the opposite side of the Galactic plane. Following the same steps (with adapted measurements), we find a fractional contamination level of only a few percent. Secondly, the velocity distribution in Fig. 1 reveals that each group contains a few stars which do not fit the general velocity profile of the groups. This closely matches the galactic field contamination estimate outlined above. Here, we chose not to remove these outliers in velocity space from our selection, since such a restriction could only be consistently applied to stars with radial-velocity measurements and not to all sources.

3. Results and discussion

3.1. Structure

Figure 2 illustrates the final member selection in Galactic Cartesian coordinates. The same distribution projected on the sky is shown in Fig. A.1. Mel 111 is located at a distance of approximately 85 pc from the Sun in the direction of the north Galactic pole. The new group is located at almost the same distance to the Galactic plane and at a similar Galactocentric radius, but about 60 pc ahead in the direction of Galactic rotation.

The Mel 111 selection reveals a flattened shape parallel to the Galactic plane, as well as a pronounced core in the cluster center. The *XY* distribution of the cluster shows a tilted ellipsoidal structure, with a length of about 60 pc and a thickness of about 25 pc. Following the discoveries of tidal tails associated with the Hyades (Röser et al. 2019; Meingast & Alves 2019), we also compared our findings for Mel 111 to the predicted tail structure as given by Chumak & Rastorguev (2006). The approximate shape of the tails is shown in the left panel of Fig. 2, which is in excellent agreement with our selected Mel 111 sources.

In contrast to Mel 111, the new group shows different morphological characteristics. Most importantly, it does not have a similarly pronounced core, which is likely the reason why it has not yet been found. Moreover, the top-down view of the new group members reveals an inhomogeneous distribution of sources, which are arranged in two parallel lanes. The two subgroups show a systematic offset in proper motions, but we do not find a significant difference in space velocities and other physical parameters. Therefore, we argue that the difference in proper motions only results from projection effects.

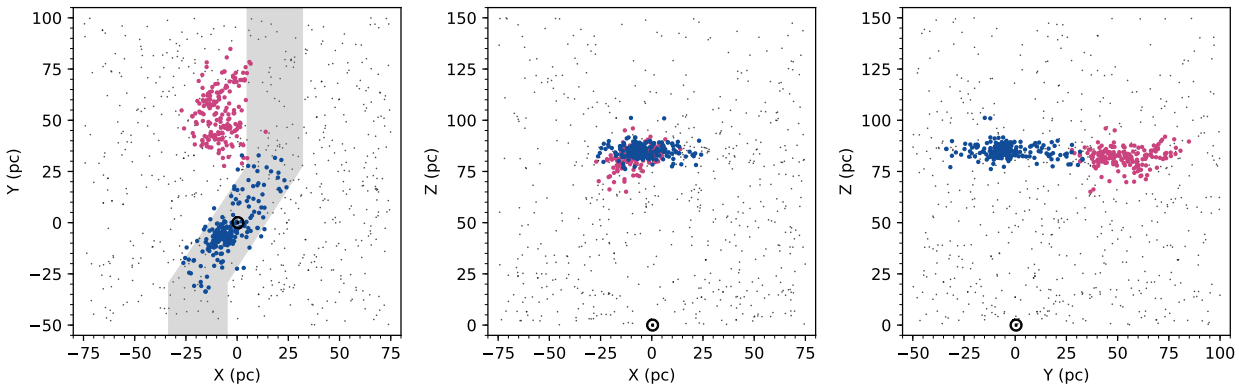

Fig. 2. Positions of the final member selection in Galactic Cartesian coordinates. The position of the Sun is indicated with the black circular symbol. The gray shaded area represents the approximate shape of the tidal tails of Mel 111 (Chumak & Rastorguev 2006). The small black dots correspond to all sources that where identified in our proper-motion clustering application but did not pass the spatial filtering.

We derive stellar masses similar to the previous entries in this paper series by interpolating isochrones for the systems (Sect. 3.2). Figure A.2 shows the resulting present-day mass functions compared to a series of initial mass functions (IMF; Kroupa 2001), which we used to estimate the birth masses of the systems. In general, we find a good match between the mass function for Mel 111 and the new group, suggesting similar current masses (affected by two-body relaxation and tidal forces). Also, we find that the present-day mass function is in overall good agreement with a 200 $M_\odot$ IMF for both systems (especially near the higher-mass end of our selection). However, the measured present-day masses of magnitude-limited samples are generally affected by incompleteness. Paper I determined the Hyades selection in this mass range to be incomplete by a factor of approximately two. Following this result, but considering the larger distances to the two groups discussed in this manuscript, we estimated the bias to result in a factor of approximately three or more, shifting the mass function closer to a 500 $M_\odot$ initial mass estimate. This estimate should be seen as a lower limit, because we did not consider mass loss caused by stellar evolution and tides. Moreover, in Sect. 3.2 we show that the new group is most likely several hundred million years younger than Mel 111. Therefore, if the initial masses of the systems were similar, the current lack of a pronounced core in the new group indicates either a different initial condition (cluster vs. association) or a very different dynamical evolution.

3.2. Age and metallicity

We present an observational HRD of our member selection in Fig. 3. Both groups show a well-defined main sequence, indicating that each group by itself comprises a coeval stellar population. While Mel 111 hosts two stars beyond the main sequence turn-off, as well as one white dwarf, all selected members of the new group are located on the main sequence. Comparing the two sequences, we find significant differences both near the upper and lower main sequence. The upper main sequence of Mel 111 is located on top of the new group, whereas this offset reverses as we follow the main sequence down to the cooler and less luminous stars, shifting Mel 111 to the bluer part.

In order to estimate the age of the two groups, we compared our selections with PARSEC isochrones (Bressan et al. 2012). Assuming solar metallicity for Mel 111 (Netopil et al. 2016), the 700 Myr isochrone appears to fit the sequence well. This is also consistent with previously published ages for Mel 111 (e.g., Tang et al. 2018; Gaia Collaboration 2018a). The upper main sequence of the new group indicates a turnoff at higher luminosities compared to Mel 111 and therefore a younger stellar age. Adjusting only the age of the isochrones, we find that a 400 Myr isochrone fits well to the upper part of the sequence. However, this adjustment does not match the observed offset near the lower main sequence.

As also metallicity generally affects the location and shape of the main sequence, we cross-matched our selection with LAMOST DR4 (Cui et al. 2012), resulting in nine matches for Mel 111 and eight matches for the new group. The mean metallicity of the matched sources is [Fe/H] = -0.117 ± 0.115 for Mel 111 and [Fe/H] = -0.003 ± 0.093 for the new group. We note here that the measured metallicity for Mel 111 is not consistent with our previous assumption of solar metallicity. This difference is likely caused by a systematic offset in the survey and we therefore only take the relative metallicity offset of ~0.1 dex between both groups into account. The 400 Myr isochrone with higher metallicity then also fits well to the lower main sequence of the new group. Clearly, more data and an improved set of models are needed to better age the new group, but the two groups were formed at different times. For the remainder of this Letter we assume their age difference to be about 300 Myr.

3.3. Kinematics and Galactic orbit

As pointed out in Sect. 2, the two groups have a very similar kinematic profile. An inspection of the Galactocentric Cylindrical velocities of both groups reveals only small differences in the radial and azimuthal velocity component ($\Delta v_r = 2.9\,\mathrm{km\,s^{-1}}$ and $\Delta v_\phi = 3.5\,\mathrm{km\,s^{-1}}$). The vertical velocity component is virtually identical. Interestingly, Mel 111, lagging behind in the Galactic rotation, is more than $3\,\mathrm{km\,s^{-1}}$ faster in v_ϕ compared to the new group. This configuration therefore indicates that Mel 111 could drift into the new group within the next few million years.

To analyze a potential encounter in more detail, we calculated the orbital motions of the groups with *Galpy* (Bovy 2015). We used a predefined axisymmetric setup for the gravitational potential of the Milky Way (MWPotential2014) which comprises a bulge, a disk, and a dark-matter-halo component; it does however not include spiral arms or molecular clouds. For a full description of the orbit, radial-velocity measurements are also required for which we added another quality criterion, limiting

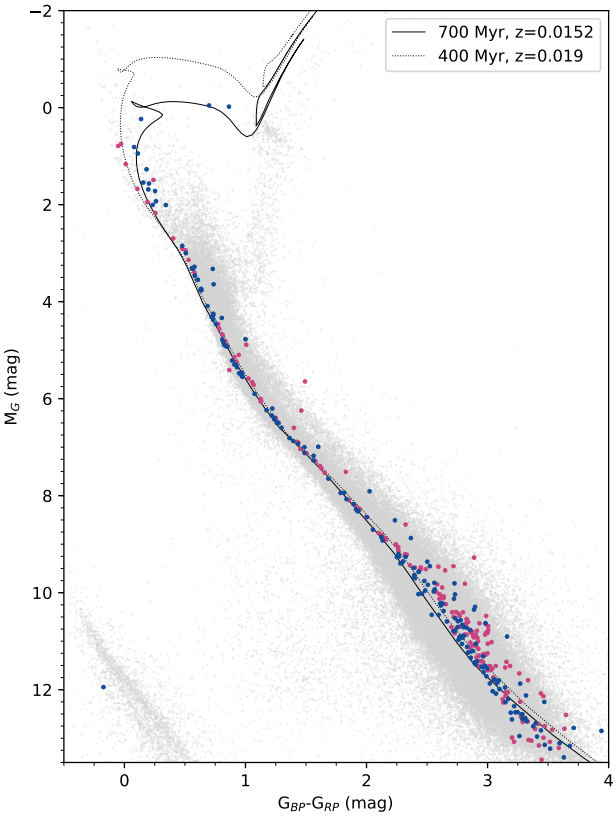

Fig. 3. Observational HRD for the member stars of Mel 111 and the new group. The solid line represents the 700 Myr PARSEC isochrone with solar metallicity and the dashed line illustrates the 400 Myr PARSEC isochrone with $z = 0.019$. The gray dots in the background are all sources in our filtered database.

the error in radial velocity to $\sigma_{rv} < 2\,\mathrm{km\,s^{-1}}$. This was applied to keep the errors of the orbit integrations at a manageable level and at the same time retain the bulk of our selection (about 90% of the sources which have radial-velocity measurements). Within these limits, we find 61 Mel 111 sources and 26 sources associated with the new group.

We estimated position errors along the integrated orbit by randomly sampling the error distribution in distance, μ_α, μ_δ, and radial velocity. Each random sample (total sample size 100) was then integrated independently, resulting in a distribution of positions for each time-step. Here, the error most significantly depends on the radial-velocity measurement. Together with the location of the groups near the Galactic north pole, this results in relatively large errors in the vertical position.

Figure 4 shows the distance between the group centers (determined as the mean position of sources) as a function of time going forward along their orbit, including the 3-σ error interval. Remarkably, the two groups continue to converge for the next few million years where we find a minimum distance of 25 pc in 13 Myr after which they start to drift apart again. Here, the escape velocity at a distance of 25 pc even for a mass estimate of 500 $M_\odot$ for Mel 111 is only $0.4\,\mathrm{km\,s^{-1}}$. Thus, the relative velocity offset between the groups is too large for a potential merging event. Nevertheless, given their spatial extent of at least 50 pc, the two systems will essentially share the same volume for about 20–30 Myr. Figure A.3 shows the position of all sources

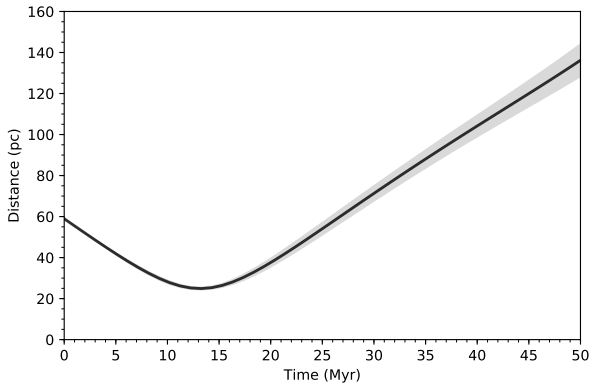

Fig. 4. Distance between Mel 111 and the new group as a function of time. The black solid line displays the mean distance and the gray shaded area corresponds to the 3-σ error. We find a minimum at $t = 13$ Myr.

in Galactic Cartesian coordinates both now and at the time of minimum distance. We also note that the orbits are integrated independently and that we did not add additional gravitational potentials for the individual groups.

This close encounter between two stellar populations encourages speculations on how often such events occur in the Galaxy. To test this, we created a simple setup of open clusters scattered across the entire Galactic disk, integrated their orbits 100 Myr forward, and calculated the average number of encounters (distance between two groups <20 pc). Specifically, we started with estimating the top-down surface density of clusters in the disk. The Webda database (Paunzen 2008) lists a total of 345 open clusters (including loose associations and moving groups) within 1 kpc. This number translates into an average of about 55 such objects per kpc^2 in the Galactic plane. Since the actual distribution of star clusters in the Galaxy is unknown and their radial distribution could even be a function of cluster age (e.g., Scheepmaker et al. 2009), we favored an isotropic setup for our toy model with a total number of 50 000 open clusters for a 30 kpc-wide disk. Furthermore, we randomly sampled the velocity distribution directly from the *Gaia* DR2 measurements of all stars in the solar neighborhood. A forward integration for 100 Myr revealed an average rate of 200 encounters per million years across the entire disk. Therefore, for our 50 000 mock clusters, each cluster should have on average one encounter every 250 Myr, indicating that such meetings of groups can happen about once per Galactic revolution.

4. Summary and conclusions

Following the previous papers in this series, we used position and velocity data provided by *Gaia* DR2 to analyze two specific overdensities in velocity space (Fig. 1). The first, more prominent peak corresponds to Mel 111, while the second overdensity, separated by only a few kilometres per second, marks a previously unknown stellar population. Moreover, these groups do not only share similar kinematics (Table A.1), but they are also currently only about 60 pc apart (Fig. 2). The spatial arrangement of the source selection for Mel 111 also shows striking similarity to theoretically predicted tidal tails. The new group however does not show a pronounced core, but instead appears to be arranged in two parallel lanes, which are not clearly separable in velocity space. A comparison of the main sequences of

the groups, taking into account metallicity differences, reveals an age of about 700 Myr for Mel 111 in agreement with previously obtained results. The age of the newly discovered group appears to be best represented by a 400 Myr isochrone (Fig. 3).

We also analyzed the kinematics of the groups in order to investigate a possible future interaction. By integrating individual orbits we find that both groups currently converge, with a minimum distance of only 25 pc between the cluster centers 13 Myr from now (Fig. 4), resulting in temporary mixing of two unrelated stellar populations (Fig. A.3) for about 20–30 Myr. The masses of the systems are however not large enough to overcome the velocity difference, preventing a merging process. A toy setup and forward integration of mock open clusters distributed across the entire Galactic disk reveals that such encounters can happen at a rate of about one per Galactic revolution for each cluster. Thus, the observed encounter between Mel 111 and the newly discovered group is probably not a unique phenomenon. This process is reminiscent, although not proof, of the multi-populations found in the massive globular clusters (Bedin et al. 2004).

Acknowledgements. We wish to thank the anonymous referee for his/her useful comments, which improved both the clarity and quality of this study. This work has made use of data from the European Space Agency (ESA) mission *Gaia* (https://www.cosmos.esa.int/gaia), processed by the *Gaia* Data Processing and Analysis Consortium (DPAC, https://www.cosmos.esa.int/web/gaia/dpac/consortium). Funding for the DPAC has been provided by national institutions, in particular the institutions participating in the *Gaia* Multilateral Agreement. This research made use of Astropy, a community-developed core Python package for Astronomy (Astropy Collaboration 2018). This research has made use of "Aladin sky atlas" developed at CDS, Strasbourg Observatory, France (Bonnarel et al. 2000). We also acknowledge the various Python packages that were used in the data analysis of this work, including NumPy (van der Walt et al. 2011), SciPy (Jones et al. 2001), scikit-learn (Pedregosa et al. 2011), scikit-image (van der Walt et al. 2014), and Matplotlib (Hunter 2007). This research has made use of the SIMBAD database operated at CDS, Strasbourg, France (Wenger et al. 2000).

References

Astropy Collaboration (Price-Whelan, A. M., et al.) 2018, AJ, 156, 123
Bedin, L. R., Piotto, G., Anderson, J., et al. 2004, Mem. Soc. Astron. It., 5, 105
Bonnarel, F., Fernique, P., Bienaymé, O., et al. 2000, A&AS, 143, 33
Bovy, J. 2015, ApJS, 216, 29
Bressan, A., Marigo, P., Girardi, L., et al. 2012, MNRAS, 427, 127
Casewell, S. L., Jameson, R. F., & Dobbie, P. D. 2006, MNRAS, 365, 447
Chumak, Y. O., & Rastorguev, A. S. 2006, Astron. Lett., 32, 446
Cui, X.-Q., Zhao, Y.-H., Chu, Y.-Q., et al. 2012, Res. Astron. Astrophys., 12, 1197
Ester, M., Kriegel, H.-P., Sander, J., & Xu, X. 1996, Proceedings of the Second International Conference on Knowledge Discovery and Data Mining, KDD'96 (San Francisco, California, USA: AAAI Press), 226
Gaia Collaboration (Prusti, T., et al.) 2016, A&A , 595, A1
Gaia Collaboration (Babusiaux, C., et al.) 2018a, A&A, 616, A10
Gaia Collaboration (Brown, A. G. A., et al.) 2018b, A&A, 616, A1
Hunter, J. D. 2007, Comput. Sci. Eng., 9, 90
Ibata, R., Malhan, K., & Martin, N. 2019, ApJ, 872, 152
Jones, E., Oliphant, T., Peterson, P., et al. 2001, SciPy: Open Source Scientific Tools for Python, see http://www.scipy.org/
Kraus, A. L., & Hillenbrand, L. A. 2007, AJ, 134, 2340
Kroupa, P. 2001, MNRAS, 322, 231
Meingast, S., & Alves, J. 2019, A&A, 621, L3
Meingast, S., Alves, J., & Fürnkranz, V. 2019, A&A, 622, L13
Netopil, M., Paunzen, E., Heiter, U., & Soubiran, C. 2016, A&A, 585, A150
Paunzen, E. 2008, Contrib. Astron. Obs. Skalnate Pleso, 38, 435
Pedregosa, F., Varoquaux, G., Gramfort, A., et al. 2011, J. Mach. Learn. Res., 12, 2825
Riedel, A. R., Blunt, S. C., Lambrides, E. L., et al. 2017, AJ, 153, 95
Röser, S., Schilbach, E., & Goldman, B. 2019, A&A, 621, L2
Scheepmaker, R. A., Lamers, H. J. G. L. M., Anders, P., & Larsen, S. S. 2009, A&A, 494, 81
Tang, S.-Y., Chen, W. P., Chiang, P. S., et al. 2018, ApJ, 862, 106
van der Walt, S., Colbert, S. C., & Varoquaux, G. 2011, Comput. Sci. Eng., 13, 22
van der Walt, S., Schönberger, J. L., Nunez-Iglesias, J., et al. 2014, PeerJ, 2, e453
Wenger, M., Ochsenbein, F., Egret, D., et al. 2000, A&AS, 143, 9

A&A 624, L11 (2019)

Appendix A: Supplementary plots and tables

Table A.1. Fundamental properties of our member selection for Mel 111 and the new group.

Property	Mel 111	New group
Candidate members	214 (67)	177 (31)
Age estimate (Myr)	700	400
RA (deg)	189.28	215.82
Dec (deg)	26.24	55.20
X (pc)	-4.01 ± 9.62	-8.34 ± 7.16
Y (pc)	-3.48 ± 12.60	52.97 ± 12.24
Z (pc)	85.05 ± 3.28	82.17 ± 4.65
d (pc)	86.67 ± 3.51	98.93 ± 7.94
rv (km s^{-1})	-0.83 ± 4.78	-6.00 ± 1.81
v_r (km s^{-1})	8.91 ± 0.61	6.04 ± 0.48
v_ϕ (km s^{-1})	226.73 ± 1.18	223.21 ± 1.07
v_z (km s^{-1})	6.06 ± 4.67	5.79 ± 1.25
U (km s^{-1})	-2.28 ± 0.71	-3.56 ± 0.63
V (km s^{-1})	-5.51 ± 1.19	-9.08 ± 1.07
W (km s^{-1})	-1.20 ± 4.67	-1.47 ± 1.25
v_α (km s^{-1})	-4.80 ± 0.41	-7.81 ± 0.50
v_δ (km s^{-1})	-3.53 ± 0.45	-1.54 ± 0.73
μ_α (mas yr^{-1})	-11.68 ± 1.10	-16.75 ± 1.97
μ_δ (mas yr^{-1})	-8.59 ± 1.13	-3.38 ± 1.76
$\sigma_{v,3D}$ (km s^{-1})	1.23	1.08

Here we provide supplementary material. Table A.1 shows fundamental properties of both groups. The parameters are average values obtained from our final source selection. The numbers in parenthesis correspond to the group members with radial-velocity measurements. As a measure of the dispersion in each parameter, we additionally quote the standard deviation of the obtained values. The comparably high dispersion of the vertical velocity component of Mel 111 can be explained by outliers in our selection and the strong dependence on radial-velocity measurements. Our determined values for Mel 111 are in excellent agreement with the literature. For example, Tang et al. (2018) estimated an age of ~800 Myr and a distance of ~86.7 pc. Riedel et al. (2017) published position and velocity coordinates of $(X, Y, Z) = (-6.706, -6.308, 87.522)$ pc and $(U, V, W) = (-2.512, -5.417, -1.204)$ km s^{-1}, and Kraus & Hillenbrand (2007) determined the mean cluster proper motion as $(\mu_\alpha, \mu_\delta) = (-11.5, -9.5)$ mas yr^{-1}.

Figure A.1 shows the distribution of our member selection in a slant orthographic projection, centered at the north Galactic pole. Figure A.2 displays the mass distribution of both groups, as well as a series of IMFs. As discussed in Sect. 3.1, both groups match well with a 200 $M_\odot$ IMF. Due to incompleteness however, we estimated their birth masses to be closer to 500 $M_\odot$, in contrast to the ~100 $M_\odot$ measured for the present-day mass of the cluster core (Casewell et al. 2006; Kraus & Hillenbrand 2007).

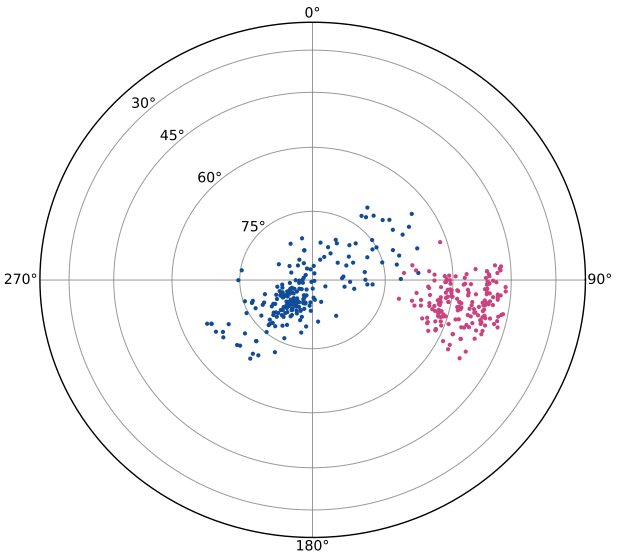

Fig. A.1. Distribution of our final member selection displayed in a slant orthographic projection with the north Galactic pole at its center.

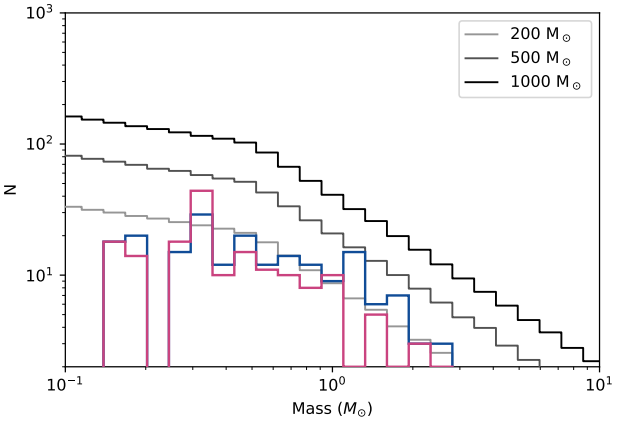

Fig. A.2. Mass functions of all member sources for both groups, with a series of IMFs on top.

Figure A.3 illustrates the positions of the member stars of Mel 111 and the new group both now and at the time of minimum distance in Galactocentric Cartesian coordinates. The mean position values are represented as dots, and the 3-σ errors are illustrated with transparent ellipses. As described in Sect. 3.1, both groups appear as flattened structures parallel to the Galactic plane. However, we do not find a similarly flat arrangement in 13 Myr. This is however caused mostly by measurement errors associated with the radial velocities.

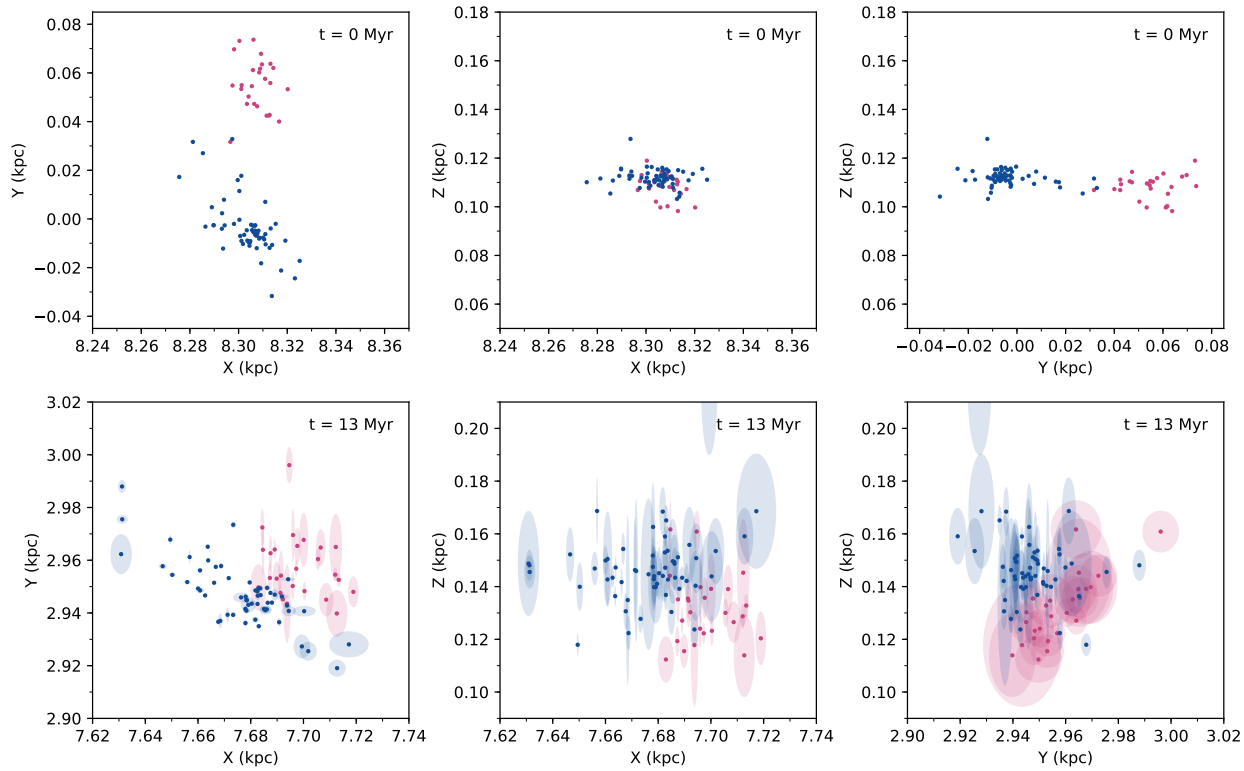

Fig. A.3. *Top row*: current position of all selected stars with radial-velocity measurements ($\sigma_{rv} < 2\,\mathrm{km\,s^{-1}}$) in the Galactocentric Coordinate frame. *Bottom row*: positions of these sources at $t = 13$ Myr. The ellipses represent the errors of orbit integration (3-σ). The large errors in the direction of Z correspond to the large errors in radial velocities and are responsible for the disappearance of the flatness of the structure parallel to the Galactic plane.

Table A.2. Top five entries: subsample of our selected Mel 111 members, five bottom sources: new group.

Gaia DR2 source_id	RA (deg)	Dec (deg)	X (pc)	Y (pc)	Z (pc)	v_α ($\mathrm{km\,s^{-1}}$)	v_δ ($\mathrm{km\,s^{-1}}$)
1259389659361730048	214.82614	26.32159	24.11	17.26	83.21	−3.9	−2.82
1259987931126020736	212.32184	26.65464	21.23	15.32	83.83	−3.96	−2.74
1260123858250996608	212.78305	27.52297	20.49	16.48	82.45	−4.12	−2.93
1260617607691437952	214.32504	28.43993	23.09	20.71	90.01	−3.71	−2.41
1285098955638193792	215.03606	30.4291	19.93	22.01	83.01	−4.93	−2.76
1489389418670610816	222.51166	42.15855	13.95	44.38	85.93	−7.59	−2.14
1497425469984297088	208.26637	41.39739	2.36	28.91	83.94	−7.96	−2.47
1498322916287022976	211.56849	41.59869	4.94	31.51	82.77	−7.57	−2.49
1499294845909337344	211.22797	42.92375	3.13	31.67	79.9	−7.75	−2.51
1503770755884281344	206.30482	46.31112	−4.2	32.06	80.3	−8.02	−2.49

Notes. The full selection, including additional columns is available at the CDS.

4. Conclusions and Outlook

This chapter provides a summary of the main results of this work. Additionally, it discusses the conclusions we can draw from it, and furthermore addresses some remaining unsolved questions and mysteries in this context, as well as how these could be approached in follow-up work.

4.1. Summary of results

The main results of this work are listed here.

1. We unveil the long-predicted tidal tails of Coma Berenices, an effect of cluster disruption due to the tidal field of the Milky Way. Our member selection of Coma Berenices reveals a pronounced core in the cluster center, as well as stars expanding from this core, flattening the group parallel to the Galactic plane.
2. We find a previously unknown moving group of stars in the velocity and spatial neighborhood of Coma Berenices. Due to its curious morphological characteristics, this group might have been difficult to detect in the past. It does not have a pronounced core, and its member stars appear to be arranged in two parallel lanes, extending over 50 pc in space.
3. We use PARSEC isochrones to estimate the age of Coma Berenices and its neighbor group to about 700 and 400 Myr, respectively. This difference in age reveals that the clusters in case represent different stellar populations, as they were formed at different times.
4. Investigation of the Galactic orbits for the next few million years shows that both groups are going to drift into each other, sharing the same Galactic volume for a few million years, after which they will drift apart again.
5. A toy setup and forward integration of mock open clusters distributed across the entire Galactic disk reveals that such encounters are not rare events in the Milky Way disk, and happen at a rate of about one per Galactic revolution for each cluster.

4.2. Discussion and future work

The wealth of data provided by *Gaia* DR2 unveils the small-scale velocity structure of our Milky Way in unprecedented detail, and the investigation of open clusters and

associations had never been so promising as during this era. The available measurements enable not only the detection of unknown stellar groups, but also contribute to increase the number of assigned member stars, and allow us to study stellar populations in various ways, e.g. their formation processes, their internal structure and kinematics, their evaporation processes, and their impact on the Galactic disk properties.

However, there are still puzzles that remain unsolved. In this work it could not yet be clarified as which kind of stellar population the previously unstudied group would be classified. As already addressed, this group is obviously no open cluster, as it clearly lacks a core in its center. Moreover, this group was probably also not formed as an association. Meingast et al. (2019) show that an association extends over 400 pc after only 120 Myr of age (Curtis et al., 2019). The group's spatial extent of only 50 pc after 400 Myr clearly indicates a different formation mechanism, or points to a possible different dynamical evolution.

A first step towards answering this question would be an improvement of the groups' age estimate. In this work, the age determination was done using PARSEC isochrones (Bressan et al., 2012) and metallicities obtained by LAMOST DR4 (Cui et al., 2012). It is widely known that evolutionary models such as isochrones are subject to big uncertainties and must be viewed with caution. Additionally, LAMOST provides metallicity measurements only for a small fraction of the stars, along with big measurement uncertainties. A useful approach to confirm or renew the age estimates obtained in this work are observations of spectra of the groups' member stars, in order to obtain lithium abundances. Lithium abundances in stars decrease with increasing age and could therefore be used as meaningful age tracers.

Further on, our membership determination method should be extended, as it is not well applicable at the outer region of Coma Berenices' core, where the stellar density strongly decreases, and the cluster member stars hardly stand out from the field stars anymore. As the abundances of elements are equal for stars that were born together, open clusters and associations appear to be chemically homogeneous (Kos et al., 2018). Therefore, chemical tagging could help to identify more member stars of these stellar populations. This method is one of the most promising future identification methods to study dispersed stellar populations, but also requires a a high number of measured abundances, and therefore a huge amount of high precision observations (Hogg et al., 2016).

The intention of our simple cluster encounter approach was to get a solid educated guess

on the number of close encounters. However, we neglected the fact that the density of star clusters within the disc decreases with distance from the Galactic center, as well as a possible age dependency on this distribution (Scheepmaker et al., 2009). Moreover, we did not take into account the influence of the rotation curve of the Galaxy on the cluster velocities. Advanced simulations could address these and more parameters, and would yield to a more sophisticated encounter estimate.

Given their small survival rate due to infant mortality in the first place, it is even more surprising that encounters of unrelated open clusters seem to be not rare events in the Milky Way disc. Advanced simulations might also be able to show how likely - if at all - merger events between open clusters occur.

In order to improve our knowledge of open clusters and associations, we need more observational data. In 2020 an early *Gaia* DR3 (EDR3) is going to be published, consisting of improved astrometric and photometric data. The full *Gaia* DR3 catalogue will be available in the second half of 2021, including - among other parameters - radial velocities for a significantly larger number of stars, due to a fainter magnitude limit. This will allow us to build on the exciting results of this work, and will open even more opportunities to investigate the stellar components of the Milky Way galaxy. With this in mind, we can look forward to to an eventful and enlightening time that will greatly contribute to our knowledge about the mysteries of the universe.

References

J. Alves, M. Lombardi, and C. J. Lada. The mass function of dense molecular cores and the origin of the IMF. *A&A*, 462(1):L17–L21, Jan 2007. doi: 10.1051/0004-6361:20066389.

C. A. L. Bailer-Jones, J. Rybizki, M. Fouesneau, G. Mantelet, and R. Andrae. Estimating distances from parallaxes IV: Distances to 1.33 billion stars in Gaia Data Release 2. *ArXiv e-prints*, art. arXiv:1804.10121, April 2018.

H. Baumgardt and P. Kroupa. A comprehensive set of simulations studying the influence of gas expulsion on star cluster evolution. *MNRAS*, 380(4):1589–1598, Oct 2007. doi: 10.1111/j.1365-2966.2007.12209.x.

Holger Baumgardt and Junichiro Makino. Dynamical evolution of star clusters in tidal fields. *MNRAS*, 340(1):227–246, Mar 2003. doi: 10.1046/j.1365-8711.2003.06286.x.

James Binney and Scott Tremaine. *Galactic dynamics*. 1987.

V. V. Bobylev and A. T. Bajkova. Kinematics of the Galaxy from a Sample of Young Open Star Clusters with Data from the Gaia DR2 Catalogue. *Astronomy Letters*, 45 (3):109–119, Mar 2019. doi: 10.1134/S1063773719030010.

S. G. Boutloukos and H. J. G. L. M. Lamers. Star cluster formation and disruption time-scales - I. An empirical determination of the disruption time of star clusters in four galaxies. *MNRAS*, 338(3):717–732, Jan 2003. doi: 10.1046/j.1365-8711.2003.06083.x.

Jo Bovy. galpy: A python Library for Galactic Dynamics. *ApJS*, 216(2):29, Feb 2015. doi: 10.1088/0067-0049/216/2/29.

Alessandro Bressan, Paola Marigo, Léo. Girardi, Bernardo Salasnich, Claudia Dal Cero, Stefano Rubele, and Ambra Nanni. PARSEC: stellar tracks and isochrones with the PAdova and TRieste Stellar Evolution Code. *MNRAS*, 427(1):127–145, Nov 2012. doi: 10.1111/j.1365-2966.2012.21948.x.

A. Castro-Ginard, C. Jordi, X. Luri, F. Julbe, M. Morvan, L. Balaguer-Núñez, and T. Cantat-Gaudin. A new method for unveiling open clusters in Gaia. New nearby open clusters confirmed by DR2. *A&A*, 618:A59, Oct 2018a. doi: 10.1051/0004-6361/201833390.

A. Castro-Ginard, C. Jordi, X. Luri, F. Julbe, M. Morvan, L. Balaguer-Núñez, and T. Cantat-Gaudin. A new method for unveiling open clusters in Gaia. New nearby open clusters confirmed by DR2. *A&A*, 618:A59, Oct 2018b. doi: 10.1051/0004-6361/201833390.

A. Castro-Ginard, C. Jordi, X. Luri, T. Cantat-Gaudin, and L. Balaguer-Núñez. Hunting for open clusters in Gaia DR2: the Galactic anticentre. *A&A*, 627:A35, Jul 2019. doi: 10.1051/0004-6361/201935531.

Bing Chen, Chris Stoughton, J. Allyn Smith, Alan Uomoto, Jeffrey R. Pier, Brian Yanny, Željko Ivezić, Donald G. York, John E. Anderson, James Annis, Jon Brinkmann, István Csabai, Masataka Fukugita, Robert Hindsley, Robert Lupton, Jeffrey A. Munn, and SDSS Collaboration. Stellar Population Studies with the SDSS. I. The Vertical Distribution of Stars in the Milky Way. *ApJ*, 553(1):184–197, May 2001. doi: 10.1086/320647.

Ya. O. Chumak and A. S. Rastorguev. Study of the nearest open clusters and the associated moving clusters by numerical simulations. *Astronomy Letters*, 32(7):446–455, Jul 2006. doi: 10.1134/S1063773706070036.

Xiang-Qun Cui, Yong-Heng Zhao, Yao-Quan Chu, Guo-Ping Li, Qi Li, Li-Ping Zhang, Hong-Jun Su, Zheng-Qiu Yao, Ya-Nan Wang, Xiao-Zheng Xing, Xin-Nan Li, Yong-Tian Zhu, Gang Wang, Bo-Zhong Gu, A. Li Luo, Xin-Qi Xu, Zhen-Chao Zhang, Gen-Rong Liu, Hao-Tong Zhang, De-Hua Yang, Shu-Yun Cao, Hai-Yuan Chen, Jian-Jun Chen, Kun-Xin Chen, Ying Chen, Jia-Ru Chu, Lei Feng, Xue-Fei Gong, Yong-Hui Hou, Hong-Zhuan Hu, Ning-Sheng Hu, Zhong-Wen Hu, Lei Jia, Fang-Hua Jiang, Xiang Jiang, Zi-Bo Jiang, Ge Jin, Ai-Hua Li, Yan Li, Ye-Ping Li, Guan-Qun Liu, Zhi-Gang Liu, Wen-Zhi Lu, Yin-Dun Mao, Li Men, Yong-Jun Qi, Zhao-Xiang Qi, Huo-Ming Shi, Zheng-Hong Tang, Qing-Sheng Tao, Da-Qi Wang, Dan Wang, Guo-Min Wang, Hai Wang, Jia-Ning Wang, Jian Wang, Jian-Ling Wang, Jian-Ping Wang, Lei Wang, Shu-Qing Wang, You Wang, Yue-Fei Wang, Ling-Zhe Xu, Yan Xu, Shi-Hai Yang, Yong Yu, Hui Yuan, Xiang-Yan Yuan, Chao Zhai, Jing Zhang, Yan-Xia Zhang, Yong Zhang, Ming Zhao, Fang Zhou, Guo-Hua Zhou, Jie Zhu, and Si-Cheng Zou. The Large Sky Area Multi-Object Fiber Spectroscopic Telescope (LAMOST). *Research in Astronomy and Astrophysics*, 12(9):1197–1242, Sep 2012. doi: 10.1088/1674-4527/12/9/003.

Jason L. Curtis, Marcel A. Agüeros, Eric E. Mamajek, Jason T. Wright, and Jeffrey D. Cummings. TESS Reveals that the Nearby Pisces-Eridanus Stellar Stream is only 120 Myr Old. *AJ*, 158(2):77, Aug 2019. doi: 10.3847/1538-3881/ab2899.

Martin Ester, Hans-Peter Kriegel, Jörg Sander, and Xiaowei Xu. A density-based algorithm for discovering clusters in large spatial databases with noise. pages 226–231. AAAI Press, 1996.

Verena Fürnkranz, Stefan Meingast, and João Alves. Extended stellar systems in the solar neighborhood. III. Like ships in the night: the Coma Berenices neighbor moving group. *A&A*, 624:L11, Apr 2019. doi: 10.1051/0004-6361/201935293.

Gaia Collaboration, C. Babusiaux, F. van Leeuwen, M. A. Barstow, C. Jordi, A. Vallenari, D. Bossini, A. Bressan, T. Cantat-Gaudin, M. van Leeuwen, A. G. A. Brown, T. Prusti, J. H. J. de Bruijne, C. A. L. Bailer-Jones, M. Biermann, D. W. Evans, L. Eyer, F. Jansen, S. A. Klioner, U. Lammers, L. Lindegren, X. Luri, F. Mignard, C. Panem, D. Pourbaix, S. Randich, P. Sartoretti, H. I. Siddiqui, C. Soubiran, N. A. Walton, F. Arenou, U. Bastian, M. Cropper, R. Drimmel, D. Katz, M. G. Lattanzi, J. Bakker, C. Cacciari, J. Castañeda, L. Chaoul, N. Cheek, F. De Angeli, C. Fabricius, R. Guerra, B. Holl, E. Masana, R. Messineo, N. Mowlavi, K. Nienartowicz, P. Panuzzo, J. Portell, M. Riello, G. M. Seabroke, P. Tanga, F. Thévenin, G. Gracia-Abril, G. Comoretto, M. Garcia-Reinaldos, D. Teyssier, M. Altmann, R. Andrae, M. Audard, I. Bellas-Velidis, K. Benson, J. Berthier, R. Blomme, P. Burgess, G. Busso, B. Carry, A. Cellino, G. Clementini, M. Clotet, O. Creevey, M. Davidson, J. De Ridder, L. Delchambre, A. Dell'Oro, C. Ducourant, J. Fernández-Hernández, M. Fouesneau, Y. Frémat, L. Galluccio, M. García-Torres, J. González-Núñez, J. J. González-Vidal, E. Gosset, L. P. Guy, J. L. Halbwachs, N. C. Hambly, D. L. Harrison, J. Hernández, D. Hestroffer, S. T. Hodgkin, A. Hutton, G. Jasniewicz, A. Jean-Antoine-Piccolo, S. Jordan, A. J. Korn, A. Krone-Martins, A. C. Lanzafame, T. Lebzelter, W. Löffler, M. Manteiga, P. M. Marrese, J. M. Martín-Fleitas, A. Moitinho, A. Mora, K. Muinonen, J. Osinde, E. Pancino, T. Pauwels, J. M. Petit, A. Recio-Blanco, P. J. Richards, L. Rimoldini, A. C. Robin, L. M. Sarro, C. Siopis, M. Smith, A. Sozzetti, M. Süveges, J. Torra, W. van Reeven, U. Abbas, A. Abreu Aramburu, S. Accart, C. Aerts, G. Altavilla, M. A. Álvarez, R. Alvarez, J. Alves, R. I. Anderson, A. H. Andrei, E. Anglada Varela, E. Antiche, T. Antoja, B. Arcay, T. L. Astraatmadja, N. Bach, S. G. Baker, L. Balaguer-Núñez, P. Balm, C. Barache, C. Barata, D. Barbato, F. Barblan, P. S. Barklem, D. Barrado, M. Barros, L. Bartholomé Muñoz, J. L. Bassilana, U. Becciani, M. Bellazzini, A. Berihuete, S. Bertone, L. Bianchi, O. Bienaymé, S. Blanco-Cuaresma, T. Boch, C. Boeche, A. Bombrun, R. Borrachero, S. Bouquillon, G. Bourda, A. Bragaglia, L. Bramante, M. A. Breddels, N. Brouillet, T. Brüsemeister, E. Brugaletta, B. Bucciarelli, A. Burlacu, D. Busonero, A. G. Butkevich, R. Buzzi, E. Caffau, R. Cancelliere, G. Cannizzaro, R. Carballo, T. Car-

lucci, J. M. Carrasco, L. Casamiquela, M. Castellani, A. Castro-Ginard, P. Charlot, L. Chemin, A. Chiavassa, G. Cocozza, G. Costigan, S. Cowell, F. Crifo, M. Crosta, C. Crowley, J. Cuypers, C. Dafonte, Y. Damerdji, A. Dapergolas, P. David, M. David, P. de Laverny, F. De Luise, R. De March, D. de Martino, R. de Souza, A. de Torres, J. Debosscher, E. del Pozo, M. Delbo, A. Delgado, H. E. Delgado, S. Diakite, C. Diener, E. Distefano, C. Dolding, P. Drazinos, J. Durán, B. Edvardsson, H. Enke, K. Eriksson, P. Esquej, G. Eynard Bontemps, C. Fabre, M. Fabrizio, S. Faigler, A. J. Falcão, M. Farràs Casas, L. Federici, G. Fedorets, P. Fernique, F. Figueras, F. Filippi, K. Findeisen, A. Fonti, E. Fraile, M. Fraser, B. Frézouls, M. Gai, S. Galleti, D. Garabato, F. García-Sedano, A. Garofalo, N. Garralda, A. Gavel, P. Gavras, J. Gerssen, R. Geyer, P. Giacobbe, G. Gilmore, S. Girona, G. Giuffrida, F. Glass, M. Gomes, M. Granvik, A. Gueguen, A. Guerrier, J. Guiraud, R. Gutié, R. Haigron, D. Hatzidimitriou, M. Hauser, M. Haywood, U. Heiter, A. Helmi, J. Heu, T. Hilger, D. Hobbs, W. Hofmann, G. Holland, H. E. Huckle, A. Hypki, V. Icardi, K. Janßen, G. Jevardat de Fombelle, P. G. Jonker, Á. L. Juhász, F. Julbe, A. Karampelas, A. Kewley, J. Klar, A. Kochoska, R. Kohley, K. Kolenberg, M. Kontizas, E. Kontizas, S. E. Koposov, G. Kordopatis, Z. Kostrzewa-Rutkowska, P. Koubsky, S. Lambert, A. F. Lanza, Y. Lasne, J. B. Lavigne, Y. Le Fustec, C. Le Poncin-Lafitte, Y. Lebreton, S. Leccia, N. Leclerc, I. Lecoeur-Taibi, H. Lenhardt, F. Leroux, S. Liao, E. Licata, H. E. P. Lindstrøm, T. A. Lister, E. Livanou, A. Lobel, M. López, S. Managau, R. G. Mann, G. Mantelet, O. Marchal, J. M. Marchant, M. Marconi, S. Marinoni, G. Marschalkó, D. J. Marshall, M. Martino, G. Marton, N. Mary, D. Massari, G. Matijevič, T. Mazeh, P. J. McMillan, S. Messina, D. Michalik, N. R. Millar, D. Molina, R. Molinaro, L. Molnár, P. Montegriffo, R. Mor, R. Morbidelli, T. Morel, D. Morris, A. F. Mulone, T. Muraveva, I. Musella, G. Nelemans, L. Nicastro, L. Noval, W. O'Mullane, C. Ordénovic, D. Ordóñez-Blanco, P. Osborne, C. Pagani, I. Pagano, F. Pailler, H. Palacin, L. Palaversa, A. Panahi, M. Pawlak, A. M. Piersimoni, F. X. Pineau, E. Plachy, G. Plum, E. Poggio, E. Poujoulet, A. Prša, L. Pulone, E. Racero, S. Ragaini, N. Rambaux, M. Ramos-Lerate, S. Regibo, C. Reylé, F. Riclet, V. Ripepi, A. Riva, A. Rivard, G. Rixon, T. Roegiers, M. Roelens, M. Romero-Gómez, N. Rowell, F. Royer, L. Ruiz-Dern, G. Sadowski, T. Sagristà Sellés, J. Sahlmann, J. Salgado, E. Salguero, N. Sanna, T. Santana-Ros, M. Sarasso, H. Savietto, M. Schultheis, E. Sciacca, M. Segol, J. C. Segovia, D. Ségransan, I. C. Shih, L. Siltala, A. F. Silva, R. L. Smart, K. W. Smith, E. Solano, F. Solitro, R. Sordo, S. Soria Nieto, J. Souchay, A. Spagna, F. Spoto, U. Stampa, I. A. Steele, H. Steidelmüller, C. A. Stephenson, H. Stoev, F. F. Suess, J. Surdej, L. Szabados, E. Szegedi-Elek, D. Tapiador, F. Taris, G. Tauran, M. B. Taylor, R. Teixeira, D. Terrett, P. Teyssand ier, W. Thuillot, A. Titarenko, F. Torra

Clotet, C. Turon, A. Ulla, E. Utrilla, S. Uzzi, M. Vaillant, G. Valentini, V. Valette, A. van Elteren, E. Van Hemelryck, M. Vaschetto, A. Vecchiato, J. Veljanoski, Y. Viala, D. Vicente, S. Vogt, C. von Essen, H. Voss, V. Votruba, S. Voutsinas, G. Walmsley, M. Weiler, O. Wertz, T. Wevers, Ł. Wyrzykowski, A. Yoldas, M. Žerjal, H. Ziaeepour, J. Zorec, S. Zschocke, S. Zucker, C. Zurbach, and T. Zwitter. Gaia Data Release 2. Observational Hertzsprung-Russell diagrams. *A&A*, 616:A10, Aug 2018a. doi: 10.1051/0004-6361/201832843.

Gaia Collaboration, D. Katz, T. Antoja, M. Romero-Gómez, R. Drimmel, C. Reylé, G. M. Seabroke, C. Soubiran, C. Babusiaux, P. Di Matteo, F. Figueras, E. Poggio, A. C. Robin, D. W. Evans, A. G. A. Brown, A. Vallenari, T. Prusti, J. H. J. de Bruijne, C. A. L. Bailer-Jones, M. Biermann, L. Eyer, F. Jansen, C. Jordi, S. A. Klioner, U. Lammers, L. Lindegren, X. Luri, F. Mignard, C. Panem, D. Pourbaix, S. Randich, P. Sartoretti, H. I. Siddiqui, F. van Leeuwen, N. A. Walton, F. Arenou, U. Bastian, M. Cropper, M. G. Lattanzi, J. Bakker, C. Cacciari, J. Casta n, L. Chaoul, N. Cheek, F. De Angeli, C. Fabricius, R. Guerra, B. Holl, E. Masana, R. Messineo, N. Mowlavi, K. Nienartowicz, P. Panuzzo, J. Portell, M. Riello, P. Tanga, F. Thévenin, G. Gracia-Abril, G. Comoretto, M. Garcia-Reinaldos, D. Teyssier, M. Altmann, R. Andrae, M. Audard, I. Bellas-Velidis, K. Benson, J. Berthier, R. Blomme, P. Burgess, G. Busso, B. Carry, A. Cellino, G. Clementini, M. Clotet, O. Creevey, M. Davidson, J. De Ridder, L. Delchambre, A. Dell'Oro, C. Ducourant, J. Fernández-Hernández, M. Fouesneau, Y. Frémat, L. Galluccio, M. García-Torres, J. González-Núñez, J. J. González-Vidal, E. Gosset, L. P. Guy, J. L. Halbwachs, N. C. Hambly, D. L. Harrison, J. Hernández, D. Hestroffer, S. T. Hodgkin, A. Hutton, G. Jasniewicz, A. Jean-Antoine-Piccolo, S. Jordan, A. J. Korn, A. Krone-Martins, A. C. Lanzafame, T. Lebzelter, W. Löffler, M. Manteiga, P. M. Marrese, J. M. Martín-Fleitas, A. Moitinho, A. Mora, K. Muinonen, J. Osinde, E. Pancino, T. Pauwels, J. M. Petit, A. Recio-Blanco, P. J. Richards, L. Rimoldini, L. M. Sarro, C. Siopis, M. Smith, A. Sozzetti, M. Süveges, J. Torra, W. van Reeven, U. Abbas, A. Abreu Aramburu, S. Accart, C. Aerts, G. Altavilla, M. A. Álvarez, R. Alvarez, J. Alves, R. I. Anderson, A. H. Andrei, E. Anglada Varela, E. Antiche, B. Arcay, T. L. Astraatmadja, N. Bach, S. G. Baker, L. Balaguer-Núñez, P. Balm, C. Barache, C. Barata, D. Barbato, F. Barblan, P. S. Barklem, D. Barrado, M. Barros, M. A. Barstow, L. Bartholomé Muñoz, J. L. Bassilana, U. Becciani, M. Bellazzini, A. Berihuete, S. Bertone, L. Bianchi, O. Bienaymé, S. Blanco-Cuaresma, T. Boch, C. Boeche, A. Bombrun, R. Borrachero, D. Bossini, S. Bouquillon, G. Bourda, A. Bragaglia, L. Bramante, M. A. Breddels, A. Bressan, N. Brouillet, T. Brüsemeister, E. Brugaletta, B. Bucciarelli, A. Burlacu,

D. Busonero, A. G. Butkevich, R. Buzzi, E. Caffau, R. Cancelliere, G. Cannizzaro, T. Cantat-Gaudin, R. Carballo, T. Carlucci, J. M. Carrasco, L. Casamiquela, M. Castellani, A. Castro-Ginard, P. Charlot, L. Chemin, A. Chiavassa, G. Cocozza, G. Costigan, S. Cowell, F. Crifo, M. Crosta, C. Crowley, J. Cuypers, C. Dafonte, Y. Damerdji, A. Dapergolas, P. David, M. David, P. de Laverny, F. De Luise, R. De March, R. de Souza, A. de Torres, J. Debosscher, E. del Pozo, M. Delbo, A. Delgado, H. E. Delgado, S. Diakite, C. Diener, E. Distefano, C. Dolding, P. Drazinos, J. Durán, B. Edvardsson, H. Enke, K. Eriksson, P. Esquej, G. Eynard Bontemps, C. Fabre, M. Fabrizio, S. Faigler, A. J. Falc a, M. Farràs Casas, L. Federici, G. Fedorets, P. Fernique, F. Filippi, K. Findeisen, A. Fonti, E. Fraile, M. Fraser, B. Frézouls, M. Gai, S. Galleti, D. Garabato, F. García-Sedano, A. Garofalo, N. Garralda, A. Gavel, P. Gavras, J. Gerssen, R. Geyer, P. Giacobbe, G. Gilmore, S. Girona, G. Giuffrida, F. Glass, M. Gomes, M. Granvik, A. Gueguen, A. Guerrier, J. Guiraud, R. Gutié, R. Haigron, D. Hatzidimitriou, M. Hauser, M. Haywood, U. Heiter, A. Helmi, J. Heu, T. Hilger, D. Hobbs, W. Hofmann, G. Holland , H. E. Huckle, A. Hypki, V. Icardi, K. Janßen, G. Jevardat de Fombelle, P. G. Jonker, Á. L. Juhász, F. Julbe, A. Karampelas, A. Kewley, J. Klar, A. Kochoska, R. Kohley, K. Kolenberg, M. Kontizas, E. Kontizas, S. E. Koposov, G. Kordopatis, Z. Kostrzewa-Rutkowska, P. Koubsky, S. Lambert, A. F. Lanza, Y. Lasne, J. B. Lavigne, Y. Le Fustec, C. Le Poncin-Lafitte, Y. Lebreton, S. Leccia, N. Leclerc, I. Lecoeur-Taibi, H. Lenhardt, F. Leroux, S. Liao, E. Licata, H. E. P. Lindstrøm, T. A. Lister, E. Livanou, A. Lobel, M. López, S. Managau, R. G. Mann, G. Mantelet, O. Marchal, J. M. Marchant, M. Marconi, S. Marinoni, G. Marschalkó, D. J. Marshall, M. Martino, G. Marton, N. Mary, D. Massari, G. Matijevič, T. Mazeh, P. J. McMillan, S. Messina, D. Michalik, N. R. Millar, D. Molina, R. Molinaro, L. Molnár, P. Montegriffo, R. Mor, R. Morbidelli, T. Morel, D. Morris, A. F. Mulone, T. Muraveva, I. Musella, G. Nelemans, L. Nicastro, L. Noval, W. O'Mullane, C. Ordénovic, D. Ordóñez-Blanco, P. Osborne, C. Pagani, I. Pagano, F. Pailler, H. Palacin, L. Palaversa, A. Panahi, M. Pawlak, A. M. Piersimoni, F. X. Pineau, E. Plachy, G. Plum, E. Poujoulet, A. Prša, L. Pulone, E. Racero, S. Ragaini, N. Rambaux, M. Ramos-Lerate, S. Regibo, F. Riclet, V. Ripepi, A. Riva, A. Rivard, G. Rixon, T. Roegiers, M. Roelens, N. Rowell, F. Royer, L. Ruiz-Dern, G. Sadowski, T. Sagristà Sellés, J. Sahlmann, J. Salgado, E. Salguero, N. Sanna, T. Santana-Ros, M. Sarasso, H. Savietto, M. Schultheis, E. Sciacca, M. Segol, J. C. Segovia, D. Ségransan, I. C. Shih, L. Siltala, A. F. Silva, R. L. Smart, K. W. Smith, E. Solano, F. Solitro, R. Sordo, S. Soria Nieto, J. Souchay, A. Spagna, F. Spoto, U. Stampa, I. A. Steele, H. Steidelmüller, C. A. Stephenson, H. Stoev, F. F. Suess, J. Surdej, L. Szabados, E. Szegedi-Elek, D. Tapiador, F. Taris, G. Tauran, M. B. Taylor, R. Teixeira,

D. Terrett, P. Teyssand ier, W. Thuillot, A. Titarenko, F. Torra Clotet, C. Turon, A. Ulla, E. Utrilla, S. Uzzi, M. Vaillant, G. Valentini, V. Valette, A. van Elteren, E. Van Hemelryck, M. van Leeuwen, M. Vaschetto, A. Vecchiato, J. Veljanoski, Y. Viala, D. Vicente, S. Vogt, C. von Essen, H. Voss, V. Votruba, S. Voutsinas, G. Walmsley, M. Weiler, O. Wertz, T. Wevers, Ł. Wyrzykowski, A. Yoldas, M. Žerjal, H. Ziaeepour, J. Zorec, S. Zschocke, S. Zucker, C. Zurbach, and T. Zwitter. Gaia Data Release 2. Mapping the Milky Way disc kinematics. *A&A*, 616:A11, Aug 2018b. doi: 10.1051/0004-6361/201832865.

M. Gieles, S. F. Portegies Zwart, H. Baumgardt, E. Athanassoula, H. J. G. L. M. Lamers, M. Sipior, and J. Leenaarts. Star cluster disruption by giant molecular clouds. *MNRAS*, 371(2):793–804, Sep 2006. doi: 10.1111/j.1365-2966.2006.10711.x.

M. Gieles, E. Athanassoula, and S. F. Portegies Zwart. The effect of spiral arm passages on the evolution of stellar clusters. *MNRAS*, 376(2):809–819, Apr 2007. doi: 10.1111/j.1365-2966.2007.11477.x.

Mark Gieles and Simon F. Portegies Zwart. The distinction between star clusters and associations. *MNRAS*, 410(1):L6–L7, Jan 2011. doi: 10.1111/j.1745-3933.2010.00967.x.

S. Gillessen, F. Eisenhauer, S. Trippe, T. Alexand er, R. Genzel, F. Martins, and T. Ott. Monitoring Stellar Orbits Around the Massive Black Hole in the Galactic Center. *ApJ*, 692(2):1075–1109, Feb 2009. doi: 10.1088/0004-637X/692/2/1075.

Simon P. Goodwin. The effect of the dynamical state of clusters on gas expulsion and infant mortality. *Ap&SS*, 324(2-4):259–263, Dec 2009. doi: 10.1007/s10509-009-0116-5.

Simon P. Goodwin and Nate Bastian. Gas expulsion and the destruction of massive young clusters. *MNRAS*, 373(2):752–758, Dec 2006. doi: 10.1111/j.1365-2966.2006.11078.x.

David W. Hogg, Andrew R. Casey, Melissa Ness, Hans-Walter Rix, Daniel Foreman-Mackey, Sten Hasselquist, Anna Y. Q. Ho, Jon A. Holtzman, Steven R. Majewski, Sarah L. Martell, Szabolcs Mészáros, David L. Nidever, and Matthew Shetrone. Chemical Tagging Can Work: Identification of Stellar Phase-space Structures Purely by Chemical-abundance Similarity. *ApJ*, 833(2):262, Dec 2016. doi: 10.3847/1538-4357/833/2/262.

J. H. Jeans. The Stability of a Spherical Nebula. *Philosophical Transactions of the Royal Society of London Series A*, 199:1–53, Jan 1902. doi: 10.1098/rsta.1902.0012.

F. J. Kerr and D. Lynden-Bell. Review of galactic constants. *MNRAS*, 221:1023–1038, Aug 1986. doi: 10.1093/mnras/221.4.1023.

N. V. Kharchenko, P. Berczik, M. I. Petrov, A. E. Piskunov, S. Röser, E. Schilbach, and R. D. Scholz. Shape parameters of Galactic open clusters. *A&A*, 495(3):807–818, Mar 2009. doi: 10.1051/0004-6361/200810407.

Janez Kos, Joss Bland-Hawthorn, Ken Freeman, Sven Buder, Gregor Traven, Gayandhi M. De Silva, Sanjib Sharma, Martin Asplund, Ly Duong, Jane Lin, Karin Lind, Sarah Martell, Jeffrey D. Simpson, Dennis Stello, Daniel B. Zucker, Tomaž Zwitter, Borja Anguiano, Gary Da Costa, Valentina D'Orazi, Jonathan Horner, Prajwal R. Kafle, Geraint Lewis, Ulisse Munari, David M. Nataf, Melissa Ness, Warren Reid, Katie Schlesinger, Yuan-Sen Ting, and Rosemary Wyse. The GALAH survey: chemical tagging of star clusters and new members in the Pleiades. *MNRAS*, 473(4): 4612–4633, Feb 2018. doi: 10.1093/mnras/stx2637.

J. M. Diederik Kruijssen. On the fraction of star formation occurring in bound stellar clusters. *MNRAS*, 426(4):3008–3040, Nov 2012. doi: 10.1111/j.1365-2966.2012.21923.x.

C. J. Lada. Star Formation in the Galaxy: An Observational Overview. *Progress of Theoretical Physics Supplement*, 158:1–23, Jan 2005. doi: 10.1143/PTPS.158.1.

Charles J. Lada and Elizabeth A. Lada. Embedded Clusters in Molecular Clouds. *ARA&A*, 41:57–115, Jan 2003. doi: 10.1146/annurev.astro.41.011802.094844.

H. J. G. L. M. Lamers and M. Gieles. Clusters in the solar neighbourhood: how are they destroyed? *A&A*, 455(2):L17–L20, Aug 2006a. doi: 10.1051/0004-6361:20065567.

H. J. G. L. M. Lamers and M. Gieles. Clusters in the solar neighbourhood: how are they destroyed? *A&A*, 455(2):L17–L20, Aug 2006b. doi: 10.1051/0004-6361:20065567.

H. J. G. L. M. Lamers, M. Gieles, N. Bastian, H. Baumgardt, N. V. Kharchenko, and S. Portegies Zwart. An analytical description of the disruption of star clusters in tidal fields with an application to Galactic open clusters. *A&A*, 441(1):117–129, Oct 2005. doi: 10.1051/0004-6361:20042241.

Henny J. G. L. M. Lamers, Holger Baumgardt, and Mark Gieles. Mass-loss rates and the mass evolution of star clusters. *MNRAS*, 409(1):305–328, Nov 2010. doi: 10.1111/j.1365-2966.2010.17309.x.

C. A. Martínez-Barbosa, A. G. A. Brown, T. Boekholt, S. Portegies Zwart, E. Antiche, and T. Antoja. The evolution of the Sun's birth cluster and the search for the solar siblings with Gaia. *MNRAS*, 457(1):1062–1075, Mar 2016. doi: 10.1093/mnras/stw006.

L. A. Martinez-Medina, B. Pichardo, A. Peimbert, and E. Moreno. On the Survival of High-altitude Open Clusters within the Milky Way Galaxy Tides. *ApJ*, 834(1):58, Jan 2017. doi: 10.3847/1538-4357/834/1/58.

Stefan Meingast and João Alves. Extended stellar systems in the solar neighborhood. I. The tidal tails of the Hyades. *A&A*, 621:L3, Jan 2019. doi: 10.1051/0004-6361/201834622.

Stefan Meingast, João Alves, and Verena Fürnkranz. Extended stellar systems in the solar neighborhood . II. Discovery of a nearby 120° stellar stream in Gaia DR2. *A&A*, 622:L13, Feb 2019. doi: 10.1051/0004-6361/201834950.

Ya O. Chumak and Alexey Rastorguev. Study of the nearest open clusters and the associated moving clusters by numerical simulations. *Astronomy Letters*, 32:446–455, 01 2006. doi: 10.1134/S1063773706070036.

J. H. Oort, F. J. Kerr, and G. Westerhout. The galactic system as a spiral nebula (Council Note). *MNRAS*, 118:379, Jan 1958. doi: 10.1093/mnras/118.4.379.

F. I. Pelupessy and S. Portegies Zwart. The evolution of embedded star clusters. *MNRAS*, 420(2):1503–1517, Feb 2012. doi: 10.1111/j.1365-2966.2011.20137.x.

Adrian M. Price-Whelan. Gala: A python package for galactic dynamics. *The Journal of Open Source Software*, 2(18), oct 2017. doi: 10.21105/joss.00388.

Siegfried Röser and Elena Schilbach. Praesepe (NGC 2632) and its tidal tails. *arXiv e-prints*, art. arXiv:1903.08610, Mar 2019.

Siegfried Röser, Elena Schilbach, and Bertrand Goldman. Hyades tidal tails revealed by Gaia DR2. *A&A*, 621:L2, Jan 2019. doi: 10.1051/0004-6361/201834608.

R. A. Scheepmaker, H. J. G. L. M. Lamers, P. Anders, and S. S. Larsen. The spatial distribution of star and cluster formation in M 51. *A&A*, 494(1):81–93, Jan 2009. doi: 10.1051/0004-6361:200811068.

Ralph Schönrich, James Binney, and Walter Dehnen. Local kinematics and the local standard of rest. *MNRAS*, 403(4):1829–1833, Apr 2010. doi: 10.1111/j.1365-2966.2010.16253.x.

Shih-Yun Tang, Xiaoying Pang, Zhen Yuan, W. P. Chen, Jongsuk Hong, Bertrand Goldman, Andreas Just, Bekdaulet Shukirgaliyev, and Chien-Cheng Lin. Discovery of Tidal Tails in Disrupting Open Clusters: Coma Berenices and a Neighbor Stellar Group. *ApJ*, 877(1):12, May 2019. doi: 10.3847/1538-4357/ab13b0.

Jacob L. Ward, J. M. Diederik Kruijssen, and Hans-Walter Rix. Not all stars form in clusters – $Gaia$-DR2 uncovers the origin of OB associations. *arXiv e-prints*, art. arXiv:1910.06974, Oct 2019.

Nicholas J. Wright. The Dynamics of OB Associations. In *20th Cambridge Workshop on Cool Stars, Stellar Systems and the Sun*, Cambridge Workshop on Cool Stars, Stellar Systems, and the Sun, page 75, Jul 2018. doi: 10.5281/zenodo.1489060.

A. Appendix

The Appendix includes additional material and information. First, I provide a German summary (Zusammenfassung) of my thesis work, which is required by the University of Vienna. Second, I provide an overview of all Figures in this work. Third, I include a reprint permission of the journal *Astronomy and Astrophysics* for my published article, which I incorporated in Chapter 3 of this thesis.

A.1. Zusammenfassung

Offene Sternhaufen und Assoziationen sind hervorragende Indikatoren zur Untersuchung der Entstehung, Entwicklung und Struktur der galaktischen Scheibe. Aufgrund ihrer geringen Geschwindigkeitsdispersion erscheinen offene Sternhaufen als kleinräumige Geschwindigkeitsstrukturen in der Milchstraße. Ihre Untersuchung liefert Einblicke in die dynamische Entwicklung von Sternhaufen in Gezeitenfeldern, in die Auflösung von Sternhaufen und Masseverlust, in die Zusammensetzung der galaktischen Feldsternpopulation und in die Massenverteilung der galaktischen Scheibe. Der zweite Gaia Datenrelease liefert astronomische Daten mit einer nie dagewesenen astrometrischen Genauigkeit. Die genauen Positions- und Geschwindigkeitsmessungen ermöglichen neue Einblicke in die Eigenschaften von Sternpopulationen in der galaktischen Scheibe und tragen dazu bei unser Wissen über die Milchstraße zu revolutionieren.

Diese Arbeit untersucht den bekannten Sternhaufen Coma Berenices und eine uns bisher unbekannte Gruppe von Sternen, die in dessen unmittelbarer Nähe liegt und ein sehr ähnliches Geschwindigkeitsprofil aufweist. Die neu entdeckte Gruppe wurde im Tangentialgeschwindigkeitsraum identifiziert, enthält mindestens 177 Sterne und erstreckt sich über 50 Parsec. Sie erscheint als abgeflachte Struktur parallel zur galaktischen Scheibe und ist etwa 300 Myr später als Coma Berenices in einem anderen Teil der Galaxie entstanden. Bemerkenswerterweise liegen die Zentren beider Gruppen in 13 Millionen Jahren so nahe, dass beide Populationen dasselbe galaktische Volumen einnehmen werden. Dies führt zu einer temporären Vermischung zweier nicht verwandter Populationen mit unterschiedlichen Metallizitäten. Nach der Phase des Zusammenlebens von etwa 20-30 Millionen Jahren werden die beiden Populationen auseinanderdriften. Wir schätzen, dass das Zusammentreffen solcher Populationen in der galaktischen Scheibe kein seltenes Ereignis ist und in der Größenordnung von einmal pro galaktischer Revolution liegt. Die Arbeit enthüllt auch die Gezeitenschweife von Coma Berenices, ein Effekt der Sternhaufen-Auflösung durch das Gezeitenfeld der Milchstraße.

A.2. List of Figures

1.1. Comparison between a globular cluster and an open cluster 2
1.2. Observational Hertzsprung-Russel diagram 3
1.3. Hubble images of the Trapezium cluster (optical and IR) 5
1.4. Stellar mass loss as a function of time for different SFEs 6
1.5. N-body simulation of an evolving cluster producing tidal tails 9
1.6. N-body simulations of open clusters in the solar neighborhood 10
1.7. Mass loss of an open cluster due to different effects 11
1.8. *Gaia* DR2 all-sky image 12
1.9. Illustration of the *Gaia* observation principle 13
1.10. UV plane of stars in the solar neighborhood 14
1.11. Small-scale velocity structure of stars in the solar neighborhood 15

2.1. Comparison of galactic and galactocentric coordinate frames 20
2.2. Illustration of the groups' galactocentric cylindrical velocities 21
2.3. Galactic orbit of Coma Berenices 22
2.4. Normal distribution sampling 23
2.5. Illustration of DBSCAN clustering method 25
2.6. Variation of DBSCAN parameters 26
2.7. Nearest neighbor criterion 27
2.8. Illustration of the contamination estimate 28

3.1. Velocity space around Coma Berenices and its neighbor group 33
3.2. Positions of the final member selection in Galactic Cartesian coordinates 34
3.3. Observational HRD with isochrones on top 35
3.4. Distance between both groups as a function of time 35
3.5. Orthographic projection of both groups 37
3.6. Mass functions of both groups 37
3.7. Positions of both groups now and in 13 Myr 38

A.3. Reprint permission

Astronomy and Astrophysics
Editor in Chief: T. Forveille

T. Forveille
Astronomy & Astrophysics
Observatoire de Paris
61, avenue de l'Observatoire
75014 Paris, France

Tel.: 33 0(1) 43 29 05 41
Fax: 33 0(1) 43 29 05 57
e-mail: aanda.paris@obspm.fr
Web: http://www.aanda.org

merging
Annales d'Astrophysique
Arkiv for Astronomi
Bulletin of the Astronomical Institutes of the Netherlands
Bulletin Astronomique
Journal des Observateurs
Zeitschrift fur Astrophysik
Bulletin of the Astronomical Institutes of Czechoslovakia

Paris, May 23, 2019

Reprint Permission

Material:
Article by Fürnkranz et al. 2019, A&A, 624, L11

To be used in:
Master thesis entitled "Like ships that pass in the night: Coma Berenices and its neighbor moving group", University of Vienna

Permission granted to:
Verena Fürnkranz
Institut für Astrophysik
Türkenschanzstraße 17
1180 Wien, Austria
verena.fuernkranz@univie.ac.at

I hold copyright on the material referred to above, and hereby grant permission for its use as requested herewith.

The article should be reproduced in the same format as that published in A&A (for example, in an appendix). In particular, the present permission rules do not allow copy-and-pasting parts of the article into the main text of the thesis.

Credit should be given as follows:
Credit: Author, A&A, vol, page, year, reproduced with permission © ESO.

Thierry Forveille
A&A Editor-in-Chief

Sponsored by Argentina, Armenia, Austria, Belgium, Bulgaria, Chile, Croatia, Czech Republic, Denmark, Estonia, Finland, France, Germany, Greece, Hungary, Italy, Lithuania, Netherlands, Norway, Poland, Portugal, Slovak Republic, Spain, Sweden, and Switzerland.
Produced and distributed by EDP Sciences for ESO.